nanomaterials

MDPI

Review

Selective Catalytic Reduction of NO_x over Perovskite-Based Catalysts Using $C_xH_y(O_z)$, H_2 and CO as Reducing Agents—A Review of the Latest Developments

Ioannis V. Yentekakis [1,2,*], Amvrosios G. Georgiadis [3], Catherine Drosou [1], Nikolaos D. Charisiou [3] and Maria A. Goula [3,*]

[1] Laboratory of Physical Chemistry & Chemical Processes, School of Chemical & Environmental Engineering, Technical University of Crete, 73100 Chania, Greece; edrosou@isc.tuc.gr
[2] Foundation for Research and Technology—Hellas/Institute of Geoenergy (FORTH/IG), Technical University of Crete, Building M1, University Campus, 73100 Chania, Greece
[3] Laboratory of Alternative Fuels and Environmental Catalysis (LAFEC), Department of Chemical Engineering, University of Western Macedonia, Koila, 50100 Kozani, Greece; amvrosiosgeorgiadis@hotmail.com (A.G.G.); ncharisiou@uowm.gr (N.D.C.)
* Correspondence: yyentek@isc.tuc.gr (I.V.Y.); mgoula@uowm.gr (M.A.G.); Tel.: +30-28210-37752 (I.V.Y.); +30-24610-68296 (M.A.G.)

Abstract: Selective catalytic reduction (SCR) is probably the most widespread process for limiting NO_x emissions under lean conditions (O_2 excess) and, in addition to the currently used NH_3 or urea as a reducing agent, many other alternative reductants could be more promising, such as $C_xH_y/C_xH_yO_z$, H_2 and CO. Different catalysts have been used thus far for NO_x abatement from mobile (automotive) and stationary (fossil fuel combustion plants) sources, however, perovskites demand considerable attention, partly due to their versatility to combine and incorporate various chemical elements in their lattice that favor deNO_x catalysis. In this work, the $C_xH_y/C_xH_yO_z$-, H_2-, and CO-SCR of NO_x on perovskite-based catalysts is reviewed, with particular emphasis on the role of the reducing agent nature and perovskite composition. An effort has also been made to further discuss the correlation between the physicochemical properties of the perovskite-based catalysts and their deNO_x activity. Proposed kinetic models are presented as well, that delve deeper into deNO_x mechanisms over perovskite-based catalysts and potentially pave the way for further improving their deNO_x efficiency.

Keywords: NO_x; perovskites; CO-SCR; H_2-SCR; hydrocarbon-SCR

Citation: Yentekakis, I.V.; Georgiadis, A.G.; Drosou, C.; Charisiou, N.D.; Goula, M.A. Selective Catalytic Reduction of NO_x over Perovskite-Based Catalysts Using $C_xH_y(O_z)$, H_2 and CO as Reducing Agents—A Review of the Latest Developments. *Nanomaterials* **2022**, *12*, 1042. https://doi.org/10.3390/nano12071042

Academic Editor: Antonio Guerrero-Ruiz

Received: 22 February 2022
Accepted: 18 March 2022
Published: 22 March 2022

Publisher's Note: MDPI stays neutral with regard to jurisdictional claims in published maps and institutional affiliations.

1. Introduction

DeNO_x—general remarks: The number of automobiles worldwide is constantly increasing, making the emission of CO, NO_x (x = 1, 2), hydrocarbons (HCs), and particulate matter (PM) in the atmosphere a major environmental problem of ever-increasing impact [1–4]. Similarly, increased energy demand for industry, home heating, etc., produced by stationary facilities, and still mainly based on fossil fuels, exacerbates the problem of air pollution in relation to these contaminants. Thereby, the regulations for emissions from stationary and mobile sources have become stringent while numerous technologies have been evolved in order to curb atmospheric pollution [1,2]. In general, heterogeneous catalysis for tackling environmental issues has been widely adopted as a low-cost, highly efficient, and selective technology for mitigating undesirable air pollutants that accompany energy production processes [5]. The prevalent heterocatalytic control technology of NO_x emissions (in excess of O_2 in the gas stream) is called selective catalytic reduction (SCR); it is an end-of-pipe, after-treatment, process that selectively reduces NO_x emissions by means of different reducing agents such as NH_3, urea, CO, H_2, or $HC/C_xH_yO_z$, using an

appropriate catalyst [1,6–14]. Although NH_3 and urea is currently the preferred choice for the SCR of NO_x applications in stationary power and chemical plants [6], reducing agents such as H_2, light hydrocarbons, and CO have recently attracted intense interest, among other reasons, due to the fact that these components usually coexist in the exhaust gases [4,5,7–15].

Dispersed on mixed oxides, typically γ-Al_2O_3-(CeO_2, La_2O_3, ZrO_2, BaO, etc.) supports, noble metals such as Rh, Pd, Ir, and Pt have been demonstrated as the most efficient and tolerant to steam-induced lattice distortion and sulfur poisoning catalysts for the control of CO, HCs and NO_x emissions [15–25] and successfully applied for years in three-way catalytic converters (TWCs) technology [2]. However, despite intensive research efforts, such noble metal catalyst formulations, although very efficient in controlling emissions of stoichiometric gasoline engines (TWC conditions), have not been yet as effective as required for the control of non-stoichiometric engines emissions in order to be applicable in the case of lean-burn gasoline and diesel engines or in stationary fossil fuel combustion processes [1,7,13]. Bearing in mind that the use of precious metals is also associated with high costs and relatively poor stability, i.e., a propensity to particle agglomeration in the case of hot spots that often occur under real driving conditions (although means and methodologies for stabilizing dispersed catalyst nanoparticles against sintering have recently been discovered [26–30]), significant efforts have been put to the development and use of alternatives such as perovskite derived catalysts, due to their unique physicochemical properties, low cost, and favorable heat stability [31–37].

Perovskite materials and their consideration in catalytic processes: Perovskites is a class of oxides that has the structural formula ABO_3, and an ideal crystalline structure described as cubic from the Pm3m space group, as shown in Figure 1 (a). On the other hand, oxides with the structural formula A_2BO_4, which are composed of alternated ABO_3 and AO layers (Figure 1 (b)), have quite similar properties to ABO_3 perovskites and are often called perovskite-like oxides [32]. Both oxide types are called hereinafter perovskites. In the structure of the perovskites, A is a large cation 12-fold coordinated with oxygen ions and located on the edge of the octahedron, while B is a smaller cation, six-fold coordinated with O^{2-} and located in the center of the octahedron (Figure 1 (a)). The tolerance factor $t = (r_A + r_O)/\sqrt{2}(r_B + r_O)$ should lie within $0.75 < t < 1.0$ in order to ensure perovskite matrix structure stability [32]. The A cation in the perovskite matrix can be an alkaline, alkaline earth, or lanthanide element, while the B cation can be an element from the 3d, 4d, or 5d configuration metals [32–44].

Perovskites are capable of partially substituting cations of A and/or B-sites by other cations with different or same valences (i.e., $A_{1-y}A'_yB_{1-x}B'_xO_{3\pm\delta}$) to adjust their redox, bulk, and surface properties [38]. That said, with an appropriate combination of A′ and B′ metals the catalytic activity of a desired reaction can be readily tuned by modifying the perovskite chemical formula [33]. Indeed, besides their high thermal stability perovskites are characterized by some additional properties that make them favorable or even unique materials for several practical applications. For example, their high mixed electronic and ionic (O^{2-}) conductivity makes them almost irreplaceable in electrocatalysis and solid oxide fuel cells (SOFCs) technology [34,45,46]; their intrinsic redox properties and oxygen ions mobility makes them beneficial materials in many heterocatalytic reaction systems, due to the sought after strong electronic metal–support interactions and oxygen ions backspillover phenomena that accompany their use. The easily adjusted acid–base properties of perovskites are also key factors that make them favorable for regulating the activity and or selectivity of many catalytic reactions, including deNO_x [1,2,31–42]. It is also worth noting that the additional ability of partially substituting A and B-sites by other cations (i.e., $A_{1-y}A'_yB_{1-x}B'_xO_{3\pm\delta}$), can provide a variety of (A, A′, B and B′ nature)-affected active sites for catalysis. For example, if La and a first series transition metal are selected for the A and B-site, respectively, high activity for NO reduction by CO can be achieved [43]. When lower valence ions are added in the A-site, which is typically occupied by a lanthanide, alkali, or alkaline earth [32,33,38–44], structural defections, as well as lattice

distortion, can be seen, leading to an improvement in terms of catalytic behavior of B cation and lattice O_2 mobility [47,48]. To illustrate this point doping with Ba^{2+}, Sr^{2+}, Rb^{1+}, and Cs^{1+} can result in the formation of structural deficiencies (i.e., anionic vacancies) and an alteration in the oxidation state of the cations enhancing the perovskite's catalytic performance.

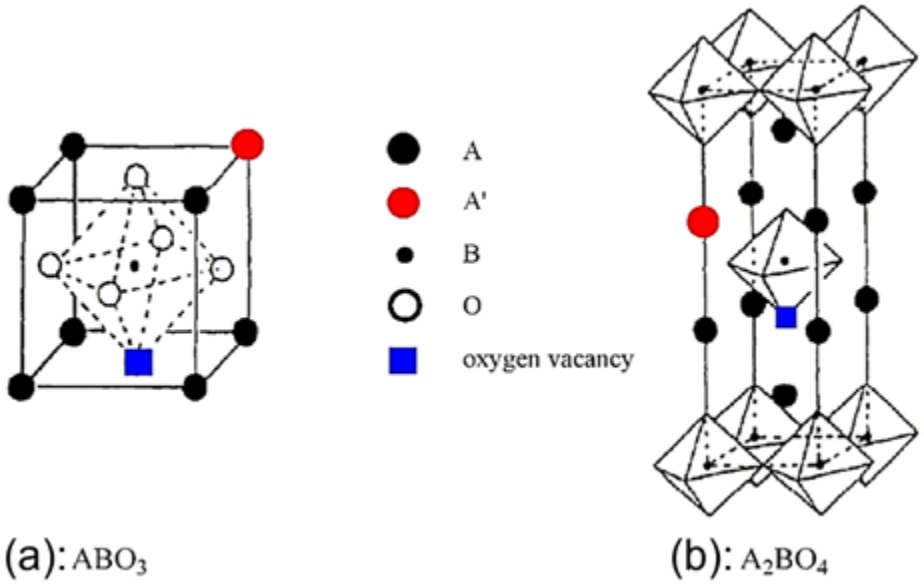

Figure 1. Ideal models of perovskite oxides with ABO_3 and A_2BO_4 structure. The red dot represents the substitution of an A-site cation by a foreign one; the blue square represents the oxygen vacancies. The oxygen symbol is not shown in the A_2BO_4 structure for simplification. Reproduced with permission from Ref. [32]. Copyright 2014, ACS.

An additional advantageous concept concerning the use of perovskite materials as metal catalyst nanoparticles supports is the so-called "redox exsolution", discovered over the last decade [49], which opened new horizons and opportunities to heterogeneous catalysts design. Pioneers in the field, Nishihata et al. [50], used a Pd–perovskite catalyst to control automotive emissions and proved that the advanced electro-catalytic properties and high durability of this class of materials can be attributed to the utilization of metal nanoparticles exsolved from perovskite oxide lattices. The authors found that Pd can reversibly move into and out of the lattice of the perovskite while undergoing oxidation and reduction (as is usually the case in exhaust gas). This movement of Pd particles seemed to inhibit the growth of Pd nanoparticles and consequently led to improved catalytic activity for long-term use. However, despite the mounting interest in this method, a thorough understanding of how the perovskite supports and driving forces are combined is still lacking [51].

The focus of the present review: The aforementioned issues, and the fact that, to the best of our knowledge, there is no other literature report that focuses exclusively on the SCR of NO_x emphasizing these three types of reducing agents (i.e., $C_xH_y/C_xH_yO_z$, H_2, CO), we have gathered herein, exhaustively, recent relevant literature results on the subject, which are thoroughly and comparatively discussed in order to shed light on current developments and new perspectives.

2. Perovskite-Catalyzed SCR of NO_x

Among the first to use perovskites in the SCR of NO_x was Buciuman et al. [47] who ascertained the superiority of the Sr-containing sample from a series of $La_{0.8}A_{0.2}MnO_3$ perovskites (A = Cs, K, Ba, Sr) studied. He et al. [52] reported a strong dependence between the degree of x substitution and catalytic activity of a $La_{1-x}Sr_xMO_3$ (M = $Co_{0.77}Bi_{0.20}Pd_{0.03}$)

perovskite under three-way catalysis (TWC) conditions, and Zhu et al. [53] showed a promising performance of $La_{2-x}Sr_xCuO_4$ perovskites for the simultaneous removal of NO and CO under similar conditions. Fino et al. [54] proposed $La_{1.8}K_{0.2}Cu_{0.9}V_{0.1}O_4$ as the best formulation for the simultaneous removal of NO_x and diesel particulate. In addition, considerable attention was paid to Cu-doped perovskites for the NO reduction by CO [43,55–59]. Noteworthy works have been carried out by Glisenti et al. [59] and Zhang et al. [43] who prepared B-site-Cu-doped perovskite catalysts to study the NO reduction by CO. With respect to A-site substitution, Ce, was thought to be the superior promoter as O_2 desorption and reducibility seemed to increase after Ce was added into the perovskite structure, although excess amounts of Ce can result in the degradation of the perovskite structure compromising the catalytic performance of the material [60–64].

As we will see in the following sections, the reduction of NO using CO as a reducing agent on perovskite catalysts has been extensively studied under conditions of absence of O_2 but very limited under conditions of excess O_2 (i.e., SCR). However, the use of hydrogen as a reducing agent of NO_x under excess O_2 conditions (H_2-SCR) has been thoroughly studied providing encouraging results [65–67].

On the other hand, historically, the use of hydrocarbons as reducing agents for SCR of NO_x (C_xH_y-SCR) in O_2-rich atmospheres has been investigated since the pioneering reports of Sato et al. [68]. In general, C_3H_6, C_3H_8, and CH_4 are considered the most common reducing agents in the C_xH_y-SCR reaction in lean conditions [48,69,70]. Nevertheless, even though C_xH_y-SCR holds great promise, it is associated with poor activity in low-temperature domains. In this regard, O_2-containing hydrocarbons (i.e., preferentially O_2-rich $C_xH_yO_z$) can be chosen as reducing agents to tackle this low-temperature inefficiency. Kucherov et al. [71] pioneered the use of ethanol as an effective reducing agent for NO reduction over Cu-ZSM-5 zeolites. The C_2H_5OH-SCR process was also investigated by Ukisu et al. [72] and Wu et al. [73] over Ag/Al_2O_3 catalysts. The latter group reported the superiority of enolic species over acetate species in generating ––CN/––NCO species and resultantly promoting the activity. However, the narrow temperature window in terms of activity, which is related to these non-perovskite-type materials, is still observed compromising the catalytic activity of the catalysts. To this end, Wang et al. [74] synthesized perovskite-based catalysts to test their activity in the $C_xH_yO_z$-SCR process under lean-burn conditions with methanol as the reducing agent.

A detailed analysis of the literature on the perovskites-catalyzed reduction of NO_x using hydrocarbons, hydrogen, or carbon monoxide as reducing agents follows. It is divided into three distinct chapters based on the means of reduction used. At the end of each chapter, a summary table is included that presents, in a comparative manner, the literature analyzed in each of the chapters.

2.1. Perovskite Catalysts in C_xH_y/$C_xH_yO_z$–SCR of NO_x

Wang et al. [74] investigated the SCR of NO by methanol (CH_3OH) using a $LaFe_{0.8}Cu_{0.2}O_3$ perovskite. The results were compared with those obtained on a Ag/Al_2O_3 reference catalyst, which is widely used in deNO_x applications. The said perovskite catalyst was prepared by a conventional citric acid (CA) complexation method, while the Ag/Al_2O_3 sample was prepared by wet impregnation. Furthermore, a high-surface-area nanoscale perovskite structure was produced by adapting the reactive grinding method (RG), which is a synthesis approach that is commonly used in metallurgy. The SCR activity tests were carried out in a tubular fixed bed quartz microreactor with a GHSV = 63,000 h^{-1}. The feed mixture comprised of 1000 ppm NO, 3000 ppm CH_3OH, 8% O_2, and He as balance gas. The catalyst physicochemical properties were explored by carrying out NO_{ads} + O_{2ads} TPD, XRD, H_2-TPR, H_2 physisorption, and isotopic exchange experiments. The $LaFe_{0.8}Cu_{0.2}O_3$ sample modified using the RG method outperformed the other tested catalysts in terms of both NO conversion and N_2 yield (Figure 2). Specifically, NO conversion of $LaFe_{0.8}Cu_{0.2}O_3$/(RG) was almost 95% at 450 °C while N_2 yield was approximately 93% as shown in Figures 2 and 3; the latter figure also shows the perovskite sites on which the

CH_3OH, O_2, and NO reactants are activated. The increased catalytic performance of $LaFe_{0.8}Cu_{0.2}O_3$/RG was attributed to the higher surface area and subsequently to the increased number of surface-active sites available (Figure 3). Furthermore, a promoting effect regarding the formation of surface bounded O_2 species was observed, probably due to the increased number of active redox sites resulting from the decrease in crystal domain size. The second-best catalyst was $LaFe_{0.8}Cu_{0.2}O_3$/CA whereas the Cu-free $LaFeO_3$/CA catalyst was third in activity order, offering maximum conversions that slightly exceeded 80% at the highest temperature (600 °C) investigated (Figure 2). The conventional Ag/Al_2O_3 catalyst performed poorly (close to inactive) for the entire temperature range under investigation (Figure 2).

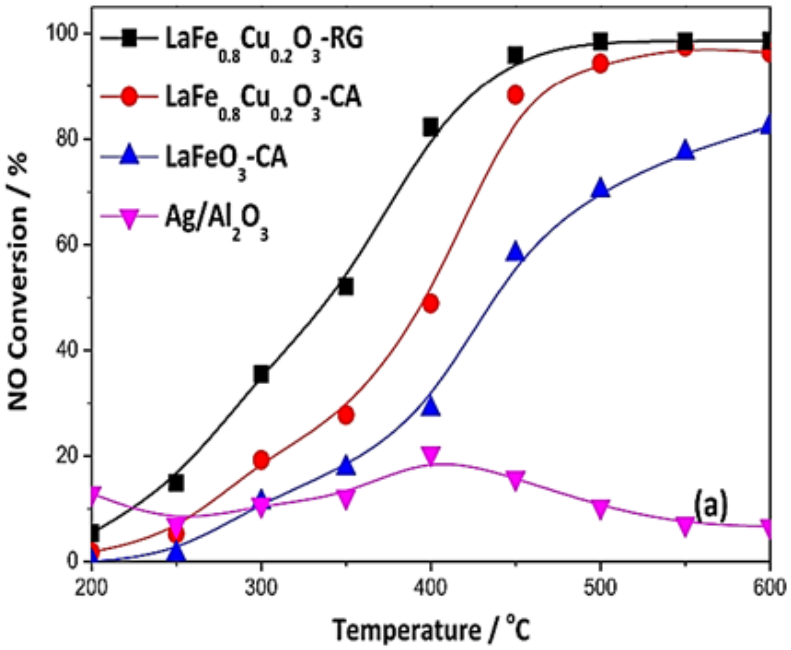

Figure 2. NO conversion performance versus temperature over different catalysts during the CH_3OH-SCR of NO_x. Reaction conditions: 1000 ppm NO, 3000 ppm CH_3OH, and 8% O_2. Reproduced with permission from Ref. [74]. Copyright 2019, Elsevier.

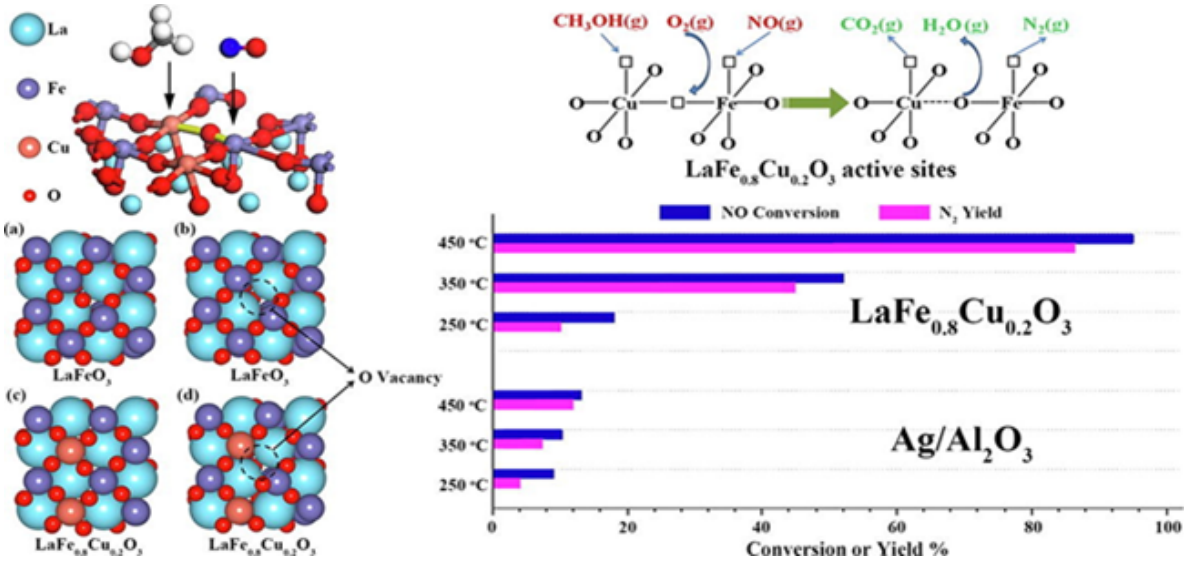

Figure 3. The deNO_x activity of $LaFe_{0.8}Cu_{0.2}O_3$ perovskite in comparison to that of Ag/Al_2O_3 catalyst during CH_3OH-SCR of NO_x. The sites for methanol, O_2, and NO adsorption/activation on the perovskite are also indicated. Reproduced with permission from Ref. [74]. Copyright 2019, Elsevier.

The deNO$_x$ performance of the catalysts was also investigated in the presence of CO_2 and H_2O in the reaction feed with the results showing an activity decrease of only ca. 10% in the presence of CO_2 in the feed and a more profound decrease (ca. 20%) in the presence of H_2O. Nevertheless, these inhibition effects were fully reversible when both CO_2 and H_2O were removed from the feed stream. Performing in situ DRIFTS studies the authors demonstrated the formation of methoxy species (−O−CH_3) over Cu-containing samples. The presence of formohydroxamic acid and carboxylate was assigned to the reaction between the adNO$_x$ nitrate/nitrite species detected on the surface of the Cu/Gr catalyst with the said methoxy species. With respect to the reference Ag/Al_2O_3 catalyst, a continuous accumulation of nitrate species over the alumina surface was noticed, upon which dehydration of methanol unequivocally ensued. This fact explained the absence of enolic intermediate of SCR over this conventional catalyst (Ag/Al_2O_3). The authors also proposed a reaction mechanism for $LaFe_{0.8}Cu_{0.2}O_3$, supported by DFT calculations; the crucial step to producing N_2 over this type of catalyst is C–N bond coupling along with the first H transfer (1.455 eV at the highest energy barrier) [74].

Teng et al. [75] conducted a joint experimental and theoretical study and proposed a system that combined enriching coal bed methane (CBM) with solar energy and SCR of NO$_x$. The basic approach was that the enriched CBM could be used as a reducing agent in SCR with a $La_{0.8}Sr_{0.2}MnO_3$ perovskite catalyst. Catalytic performance results showed that the CH_4-SCR system exhibited the highest NO conversion (80%) with recorded outlet NO concentrations below 20 mg·m^{-3}. Regarding the numerical simulations, the Navier–Stokes equations were used with the hypothesis that density difference, caused by a temperature gradient, was the key parameter. The authors argued that the temperature gradient, caused by the exploitation of solar energy, can enrich CBM and subsequently more CH_4 can be accumulated at the zone at increased temperature. In this regard, when the temperature difference was 150, the number of enriching units was estimated to be 200, which corresponded to a final CH_4 mole fraction of 0.8.

The same group [76] used CH_4 as a reductant to study the SCR of NO, though this time over an a-Al_2O_3-supported $La_{0.8}Sr_{0.2}MnO_3$ perovskite-type catalyst. The precursor was prepared by a conventional sol–gel method, while the supported $La_{0.8}Sr_{0.2}MnO_3$/a-Al_2O_3 catalyst was synthesized by a co-impregnation method. The perovskite structure of $La_{0.8}Sr_{0.2}MnO_3$/a-Al_2O_3 was corroborated by XRD and SEM analysis. The inlet flue gas in the fixed bed reactor contained excess methane (CH_4/NO = 1.2:1000 ppm NO, 1200 ppm CH_4, 0–10% of O_2 and N_2 as carrier gas) to facilitate NO reduction, where the effect of temperature (600–900 °C) and resident time (τ = 1.0 sec, 1.6 sec, 2.2 sec) was evaluated. It was shown that, in the absence of O_2, methane can effectively convert NO (i.e., above 90%) over the $La_{0.8}Sr_{0.2}MnO_3$/a-Al_2O_3. On the other hand, in the presence of O_2, the NO conversion was positively correlated with resident time. A positive correlation was also observed between NO conversion and temperature when the O_2 content ranged from 0% to 3%. Furthermore, at high reaction temperatures, moderate O_2 concentration was found to promote the NO reduction by filling the O_2 vacancies in the lattice. Interestingly, the supported catalyst had a decent performance for the broadest range of O_2 concentrations, while it outreached 90% of NO conversion when the O_2 concentration ranged from 4% to 6%. The authors concluded that the optimal experimental condition was: 2.2 s of residence time, 4–6% of O_2 concentration in feed gas, and 800 °C of reaction temperature.

Giroir-Fendler et al. [77] evaluated the catalytic activity of $LaMnO_3$ and partially substituted $La_{0.8}A_{0.2}MnO_3$ (A = K, Sr) perovskites for the SCR of NO using decane ($C_{10}H_{22}$) as reductant, as well as NO oxidation and $C_{10}H_{22}$ oxidation. A 2 wt% Pt/SiO_2 sample was also used as a reference catalyst for comparison. The perovskite materials were synthesized by a complexation route. The gas mixture comprised of 400 ppm(v) NO, 240 ppm(v) $C_{10}H_{22}$, 1.5 vol% H_2O, and 9 vol% O_2 (WGHSV = 36,000 mL·g^{-1}·h^{-1}) resembling a diesel exhaust gas, and the light-off behavior of the catalytic systems was acquired in the temperature range 100 to 500 °C (Figure 4). With respect to the reference 2 wt% Pt/SiO_2 catalyst, 50% conversion was achieved at 180 °C which was 50 °C higher compared to the corresponding

temperature shown during the $C_{10}H_{22}$ oxidation experiments (Figure 4A). The presence of NO did not affect the oxidation of $C_{10}H_{22}$ when the $La_{0.8}Sr_{0.2}MnO_3$ catalyst was used (Figure 4B). Catalytic tests in the absence of NO at 190 °C provided a similar T_{50} value. Interestingly, $C_{10}H_{22}$ conversion for both Pt/SiO_2 and $La_{0.8}Sr_{0.2}MnO_3$ catalysts reached 100% at 200 °C (Figure 4).

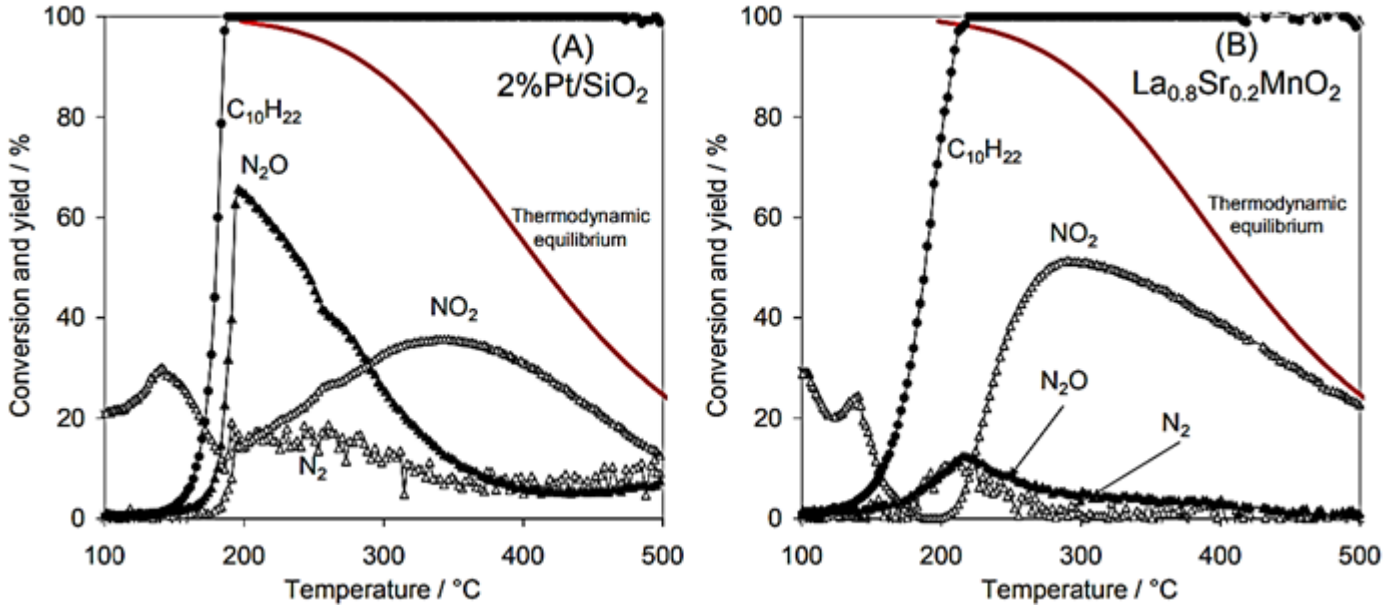

Figure 4. Reactant ($C_{10}H_{22}$) conversion and product (N_2, N_2O, NO_2) yields for Pt/SiO_2 (**A**) and $La_{0.8}Sr_{0.2}MnO_3$ (**B**) catalysts (feed gas: 400 ppm NO, 240 ppm $C_{10}H_{22}$, 1.5 vol% H_2O, and 9 vol% O_2). Reproduced with permission from Ref. [77]. Copyright 2014, Elsevier.

A closer look at the behavior of Pt/SiO_2 catalyst under SCR conditions (Figure 4A) shows that both reduction of NO to N_2O and $C_{10}H_{22}$ oxidation initiated at the same temperature, while the maximum N_2O yield (i.e., 65%) was obtained at 195 °C when the conversion of $C_{10}H_{22}$ was 100%. The amount of N_2 produced was lower compared to that of N_2O, both reaching maximum yields of 18% and 65%, respectively, at ~200 °C. Exceeding 200 °C, N_2 and N_2O yields dropped, though, NO conversion to NO_2 showed an increasing trend and reached a maximum of 37% at 370 °C. The maximum NO_2 yield was lower and shifted to higher temperatures when NO oxidation took place in the absence of $C_{10}H_{22}$. In addition, the NO_2 yield was below the thermodynamic equilibrium curve even at the highest temperature of 500 °C reached (Figure 4A). The $La_{0.8}Sr_{0.2}MnO_3$ catalyst showed a relatively different catalytic behavior than Pt/SiO_2. A less competitive relationship between NO and $C_{10}H_{22}$ was observed for temperatures lower than 200 °C, and thereby NO conversion was not favored toward $C_{10}H_{22}$ oxidation. The maximum values of N_2 and N_2O yields (almost 13%) at 210 °C were obtained when the conversion of $C_{10}H_{22}$ was 100%. NO_2 production started at 200 °C and reached a maximum value of 50% at 290 °C. Regarding the maximum yield of NO_2, it was lower compared to that of the NO oxidation experiment in the absence of $C_{10}H_{22}$, however, it was recorded at almost the same temperature ca. 285–290 °C. The fact that the NO/$C_{10}H_{22}$ system exhibited lower maximum NO_2 yield was ascribed to the parallel oxidation reactions of $C_{10}H_{22}$ and NO over different redox systems (Mn^{3+}/Mn^{2+} and/or Mn^{4+}/Mn^{3+}). The said redox systems were considered as the active species participating in the Mars–van Krevelen mechanism, which is a widely accepted mechanism for hydrocarbons oxidation using mixed oxide catalysts [78,79]. The perovskite ($La_{0.8}Sr_{0.2}MnO_3$ catalyst) showed better NO → NO_2 oxidation activity and thus allowed a closer approximation of the thermodynamic equilibrium of this reaction compared to the Pt-based catalyst (Figure 4). Finally, the authors concluded that the $La_{0.8}Sr_{0.2}MnO_3$

perovskite could be a promising alternative, noble metal-free catalyst for NO_x emission control (Figure 5). Table 1 synopsizes the main literature studies analyzed in Section 2.1.

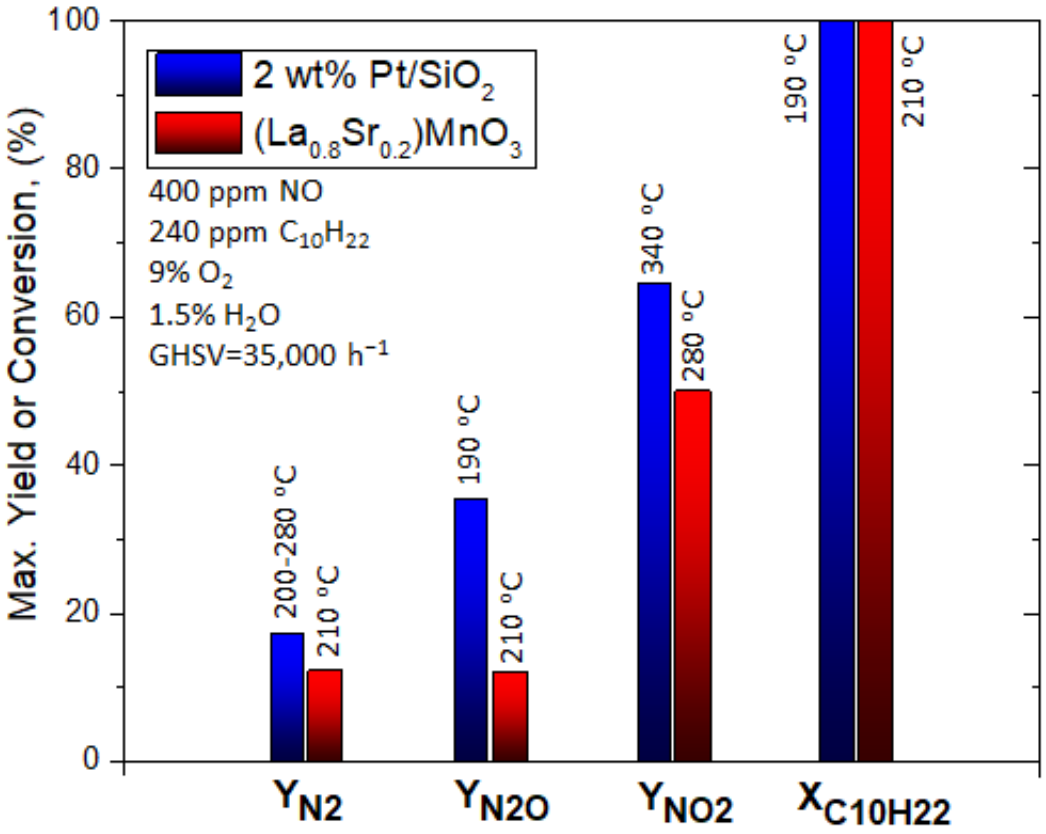

Figure 5. Comparison of the maximum N_2, N_2O, NO_2 yields, and NO conversions and the corresponding temperatures these maxima appeared at for the $C_{10}H_{22}$-SCR of NO_x over a noble metal-based catalyst and a noble metal-free perovskite catalyst. Reproduced with permission from ref. [77]. Copyright 2014, Elsevier.

Table 1. Perovskite-catalyzed $H_xC_y(O_z)$-SCR of NO_x representative studies.

Catalyst	Reaction Feed Conditions					Achievements			Ref.
	NO (%)	HC (%)	O_2 (%)	Other (%)	WGHSV ($mL \cdot g^{-1} \cdot h^{-1}$)	X_{NO} (%)	at T (°C)	S_{N2} (%)	
Perovskite and NM/perovskite catalysts									
$LaFe_{0.8}Cu_{0.2}O_3$-RG	0.1	0.3 (CH_3OH)	8	-	30,000	> 90	> 430	n/a	[74]
$LaFe_{0.8}Cu_{0.2}O_3$-CA	0.1	0.3 (CH_3OH)	8	-	30,000	> 90	> 475	n/a	[74]
$LaFeO_3$-CA	0.1	0.3 (CH_3OH)	8	-	30,000	> 80	> 575	n/a	[74]
$La_{0.8}Sr_{0.2}MnO_3/\alpha$-$Al_2O_3$	0.1	0.12 (CH_4)	0	-	1636 h^{-1} (GHSV)	> 90	> 875	n/a	[76]
$La_{0.8}Sr_{0.2}MnO_3/\alpha$-$Al_2O_3$	0.1	0.12 (CH_4)	5	-	1636 h^{-1} (GHSV)	96	800	n/a	[76]
$La_{0.8}Sr_{0.2}MnO_3$	0.4	0.24 ($C_{10}H_{22}$)	9	1.5 (H_2O)	36,000	20–65	200–275	13 (max at 210 °C)	[77]
Conventional, supported on oxide supports NM catalysts									
2wt%Pt/SiO_2	0.4	0.24 ($C_{10}H_{22}$)	9	1.5 (H_2O)	36,000	> 90	200–250	18 (max at 200 °C)	[77]
0.5wt%Pt/γ-Al_2O_3	0.1	0.1 (C_3H_6)	5	-	180,000 *	> 50	300–400	40 (at 300 °C)	[7]
0.5wt%Pt(1.6wt%Na)/γ-Al_2O_3	0.1	0.1 (C_3H_6)	5	-	53,485 *	> 50	225–375	75 (at 225 °C)	[7]

* The same contact time of the reactants with the catalyst active sites was imposed in these two cases by adjusting WGHSV.

2.2. Perovskite Catalysts in H_2-SCR of NO_x

Efstathiou and co-workers [9] using a ceramic method prepared a $La_{0.7}Sr_{0.2}Ce_{0.1}FeO_3$ solid in which the major crystal phases detected by XRD were $LaFeO_3$ and $SrFeO_{3-x}$ perovskite structures and the oxidic phases CeO_2 and Fe_2O_3 (i.e., not a pure perovskite but a mixed oxide material). The material was used as support for the preparation of a 1 wt% Pt content catalyst, by wet impregnation (1 wt% $Pt/La_{0.7}Sr_{0.2}Ce_{0.1}FeO_3$), while counterpart catalysts, namely 1 wt% Pt content Pt/CeO_2, Pt/Fe_2O_3, and Pt/SiO_2, were also prepared for the sake of comparison. The H_2-SCR deNO_x performance of the $Pt/La_{0.7}Sr_{0.2}Ce_{0.1}FeO_3$ catalyst, using a 0.25% NO/1% H_2/5% O_2/balance He at a WGHSV of 40,000 $mL \cdot g^{-1} \cdot h^{-1}$ (GHSV = 80,000 h^{-1}), found to transcend that of the other tested catalysts: a maximum NO conversion of 83% with a N_2-selectivity as high as 93% was achieved at 150 °C; corresponding maximum values for Pt/SiO_2, Pt/CeO_2, and Pt/Fe_2O_3 catalysts were X_{NO} = 82%/S_{N2} = 65% (at 120 °C), X_{NO} = 82%/S_{N2} = 43% (at 150 °C), and X_{NO} = 16%/S_{N2} = 5% (at 200 °C), respectively. Notably, for the optimal $Pt/La_{0.7}Sr_{0.2}Ce_{0.1}FeO_3$ catalyst, the addition of 5% H_2O in the feed stream at 140 °C resulted in some widening of the operating temperature window with considerable NO conversion and N_2-selectivity values, while no degradation effects were observed on its stability for 20 h time-on-stream.

Luo et al. [80] prepared, via a sol–gel method, a series of $LaNi_{1-x}Fe_xO_3$ (x = 0.0, 0.2, 0.4, 0.7, 1.0) perovskites to study the SCR of NO_x by H_2 at temperatures between 200 and 400 °C in a fixed bed reactor (500 mg catalyst) using a 500 ppm NO, 3.5 vol% H_2, 8 vol% O_2 (balance N_2) gas feed composition with a total flow rate of 600 mL min^{-1}. Sulfur-aging and regeneration treatments were also involved in their study. They found that Fe-doping of the base $LaNiO_3$ perovskite results in a better NO_x removal (Figure 6), and high structural stability.

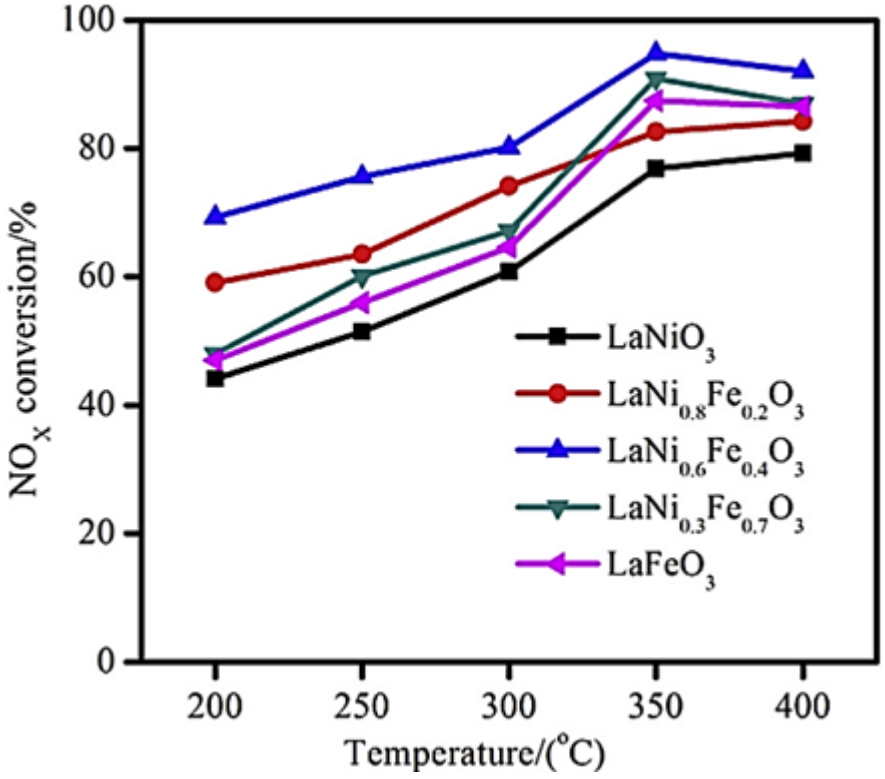

Figure 6. Effect of temperature on NO_x conversion efficiency of $LaNi_{1-x}Fe_xO_3$ perovskite catalysts during H_2-SCR of NO_x. Reproduced with permission from Ref. [80]. Copyright 2014, Elsevier.

H_2-TPR analysis showed that partial substitution of Ni by Fe results in better reducibility of nickel particles ($Ni^{3+} \rightarrow Ni^{2+}$), which in turn play a critical role in promoting NO-SCR. The perovskite $LaNi_{0.6}Fe_{0.4}O_3$ with the best reducibility characteristics was the best

overall in deNO$_x$ performance (Figure 6). Regarding perovskite stability, N_2 physisorption and SEM analysis showed that the partial substitution of nickel with appropriate amounts of Fe can lead to enhanced surface area as well as thermal stability. Finally, the bulk $LaNiO_3$ and $LaNi_{0.6}Fe_{0.4}O_3$ were tested toward their sulfur resistance and regeneration ability. Results showed that the presence of SO_2 resulted in lower NO_x conversion in both cases. However, both samples were capable of being regenerated after 12-h long H_2 treatment. XPS results (Figure 7) suggested the predominance of sulfate species formed on the active nickel components, whereas the addition of Fe significantly affected the sulfation process, leading to enhanced sulfur resistance.

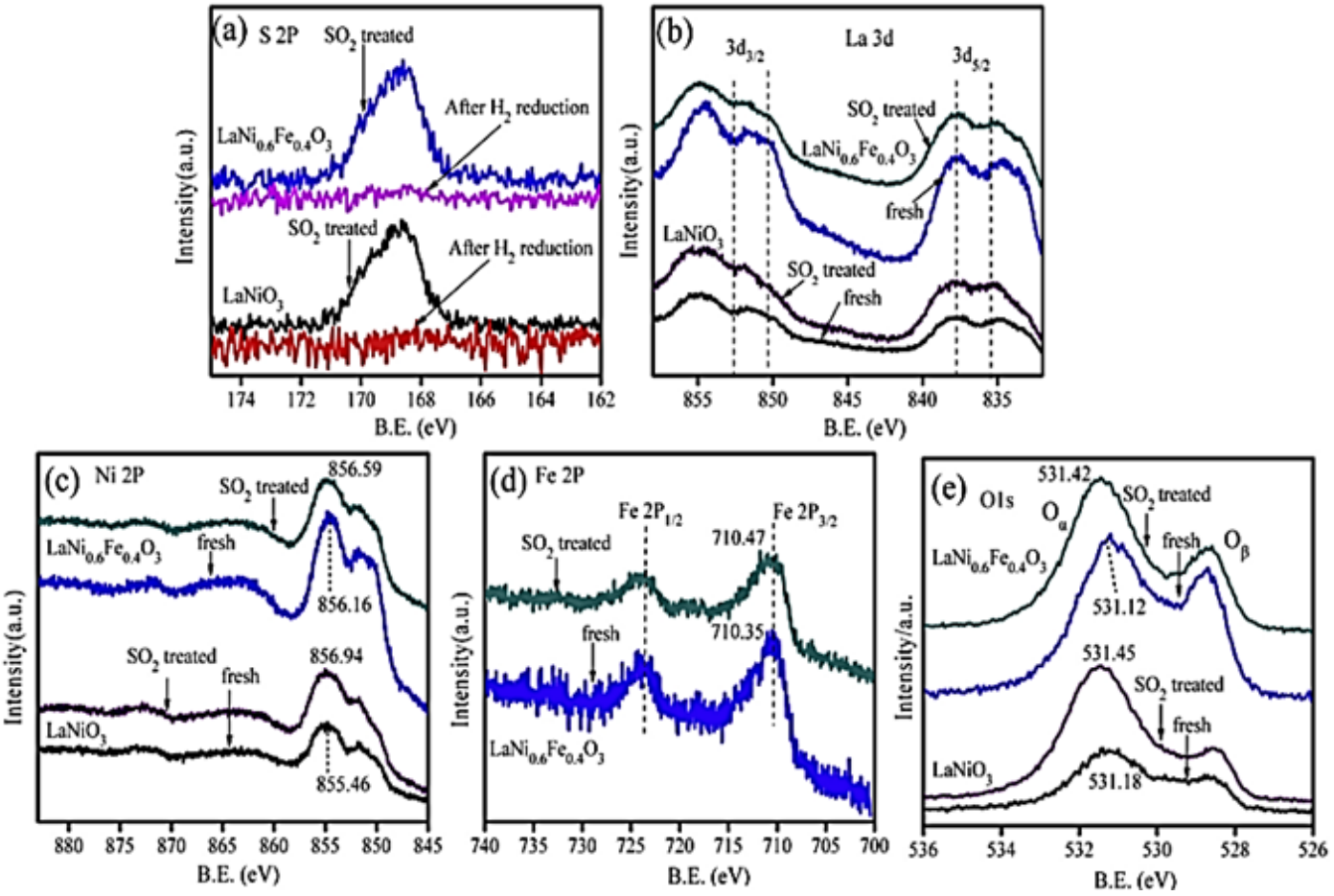

Figure 7. XPS analysis of $LaNi_{1-x}Fe_xO_3$ in the (**a**) S 2p, (**b**) La 3d, (**c**) Ni 2p, (**d**) Fe 2p, and (**e**) O 1s. Reproduced with permission from Ref. [80]. Copyright 2014, Elsevier.

Using a cost-effective solution combustion synthesis (SCS) method, Furfori et al. [81] prepared a series of perovskites and Pd-promoted (via wet impregnation) perovskite-type catalysts belonging to the $LaFeO_3$ group in order to evaluate their catalytic performance and decipher H_2-SCR of NO_x mechanisms in the absence and presence of O_2. The synthesized catalysts were $La_{0.8}Sr_{0.2}FeO_3$, $Pd/La_{0.8}Sr_{0.2}FeO_3$, $La_{0.8}Sr_{0.2}Fe_{0.9}Pd_{0.1}O_3$, $La_{0.7}Sr_{0.2}Ce_{0.1}FeO_3$, $Pd/La_{0.7}Sr_{0.2}Ce_{0.1}FeO_3$, $La_{0.7}Sr_{0.2}Ce_{0.1}Fe_{0.9}Pd_{0.1}O_3$, and bulk $LaFeO_3$; Figure 8 shows a field emission scanning electron micrograph of the $La_{0.8}Sr_{0.2}FeO_3$ sample appearing as a very foamy structure, a structure that was found to be representative of all perovskites prepared by the SCS method with a specific surface area, ~10 $m^2 \cdot g^{-1}$ on average. The catalytic tests performed in a fixed bed reactor at the temperature range of 25–400 °C, using a gas feed consisted of 1000 ppm NO, 4000 or 10,000 ppm H_2, 0 or 5% O_2, balance He, at WGHSVs = 180,000, 270,000 and 360,000 $mL \cdot g^{-1} \cdot h^{-1}$ (GHSV = 20,000, 30,000, and 40,000 h^{-1}). In the absence of O_2 in the feed stream, the most promising catalyst that outperformed all

other catalysts was found to be $La_{0.8}Sr_{0.2}Fe_{0.9}Pd_{0.1}O_3$ (Figure 9), which was then further studied in the presence of 5% O_2 at three different WGHSVs, and at a higher H_2 concentration in the feed (10,000 ppm). Up to 75% NO conversion toward N_2 at a temperature as low as 125 °C for WGHSV = 180,000 $mL \cdot g^{-1} \cdot h^{-1}$ was achieved. For the highest space velocity value, the maximum NO conversion to N_2 was reduced to ~55% while the corresponding temperature was shifted to a value ~10 °C higher. As the temperature increased, the selectivity to N_2 gradually decreased due to the favorable formation of N_2O and NO_2, a behavior typical of SCR processes. Regarding the $deNO_x$ reaction mechanism, H_2-TPR and other characterization results allowed the authors to conclude that both the availability of oxygen vacancies (suitable for NO adsorption) and the reducibility of the B-sites play a critical role in the catalytic activity of the perovskites. Finally, the authors stated that the results, although promising, do not yet meet industry demands.

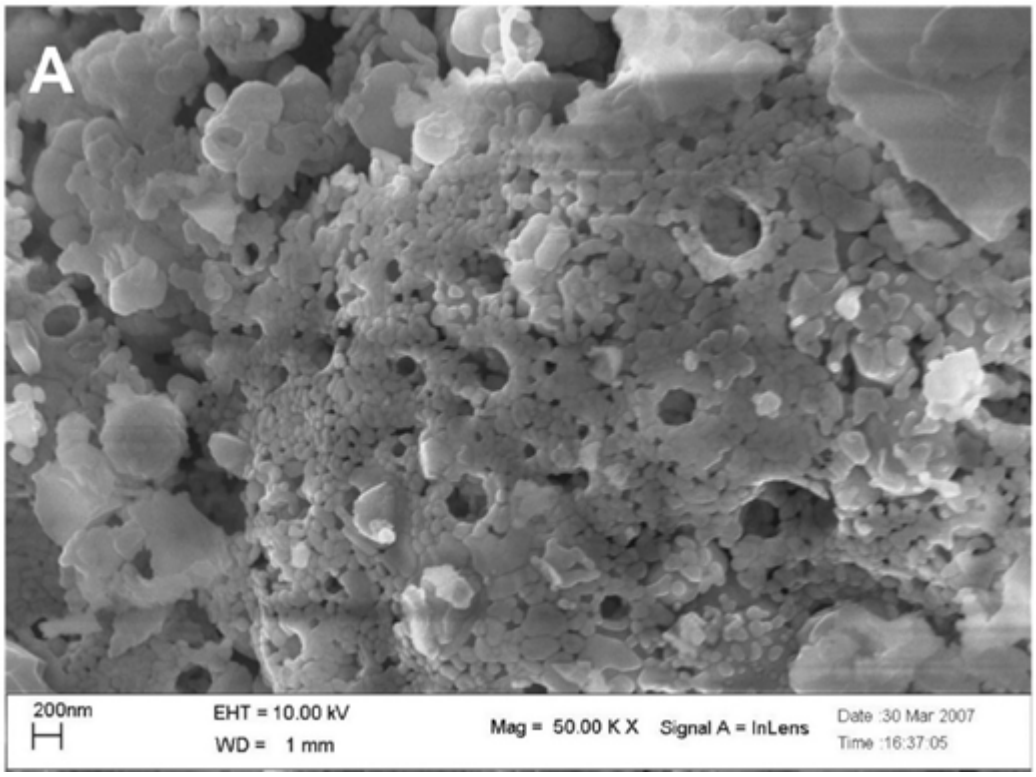

Figure 8. Field emission SEM micrograph of the $La_{0.8}Sr_{0.2}FeO_3$ catalyst crystals. Reproduced with permission from Ref. [81]. Copyright 2010, Elsevier.

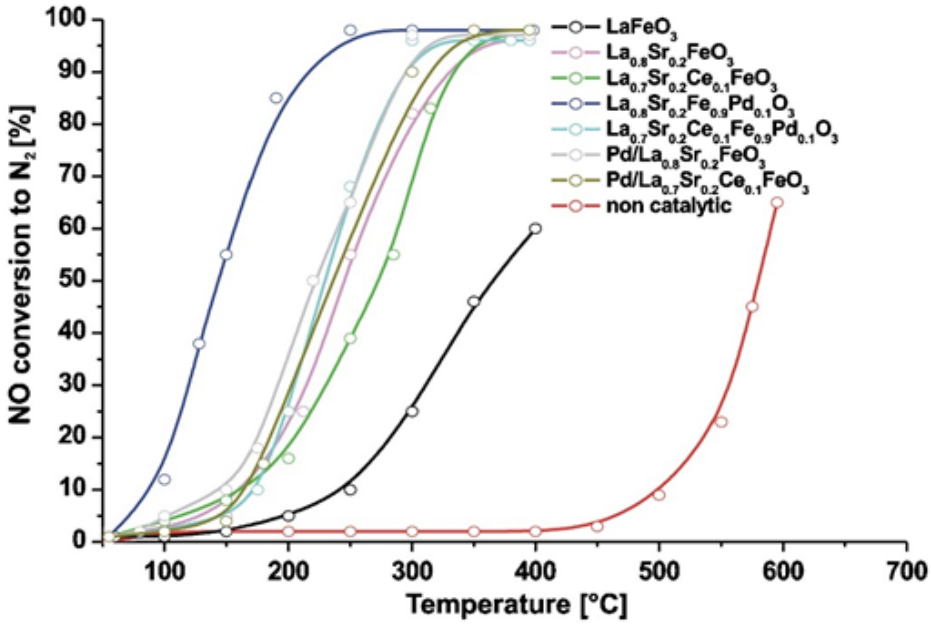

Figure 9. Comparison of the NO conversion light-off performance of all synthesized perovskite-type catalysts under 1000 ppmv NO, 4000 ppmv H_2, 0% O_2, balance He, WGHSV = 180,000 $mL \cdot g^{-1} \cdot h^{-1}$ feed conditions. Reproduced with permission from Ref. [81]. Copyright 2010, Elsevier.

Mondragon Rodriguez and Saruhan [67] studied the effect of Fe/Co-ratio on the phase composition of $LaFe_{0.95-x}Co_xPd_{0.05}O_3$ (x = 0.475, 0.4, 0.3) perovskite catalysts and then evaluated their behavior with respect to H_2-SCR of NO_x. The catalysts under consideration were prepared by the so-called citrate method. Three different feed stream composition protocols were adopted during catalyst evaluation tests in a tubular fixed bed reactor operated at 1 bar. In the first one the feed gas comprised of 0.072% NO, 5% O_2, 1% H_2, He balance. The second experimental protocol included the addition of 7.2% H_2O and 7.2% CO_2 to the mixture (0.072% NO, 5% O_2, 1% H_2, 7.2% H_2O), while the third one included the addition of 0.25% CO instead of H_2O, and CO_2 (0.072% NO, 5% O_2, 1% H_2, 0.25% CO). The WGHSV in all experiments was kept at 55,000 $mL \cdot g^{-1} \cdot h^{-1}$ and the reaction temperature ranged from 50 to 400 °C. All tested samples were characterized using the TPR, EDS, FESEM, XPS, XRD, and DSC techniques. Results from the first experimental protocol suggested that $LaFe_{0.475}Co_{0.475}Pd_{0.05}O_3$ and $LaFe_{0.65}Co_{0.3}Pd_{0.05}O_3$ exhibited the best (i.e., 79% NO conversion at 180–230 °C) and second-best (i.e., 74% NO conversion at 200 °C) catalytic performance, respectively. Representative field emission SEM images of these two materials are depicted in Figure 10.

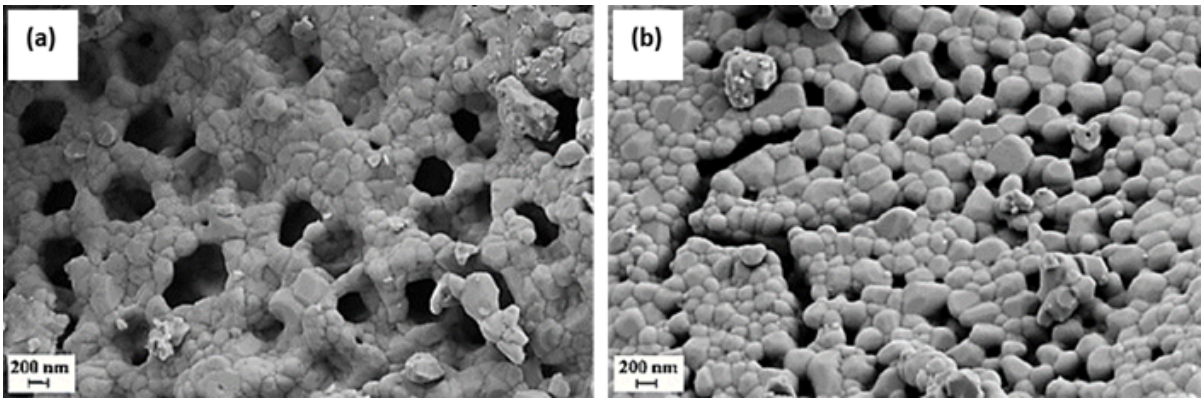

Figure 10. SEM images of the perovskite surface $LFC_{(0.3)}$-Pd (**a**) and $LFC_{(0.475)}$-Pd (**b**) after calcination in air at 900 °C/3 h. Reproduced with permission from Ref. [67]. Copyright 2010, Elsevier.

Figure 11a shows that the NO_x conversion of $LaFe_{0.475}Co_{0.475}Pd_{0.05}O_3$ and $LaFe_{0.65}Co_{0.3}Pd_{0.05}O_3$ followed a typical volcano-type behavior [67], indicating the existence of competing redox reactions which might entail the dissociation of NO into adsorbed N and O species, as also proposed by Burch and Coleman [82] upon investigating the H_2-SCR of NO_x over platinum group metal catalysts dispersed on traditional oxide supports. The optimum operating temperature was between 200 °C and 250 °C (Figure 11a). By decreasing the Co-content of the La-containing perovskites, the selectivity of N_2 shifted to higher temperatures (Figure 11b). Nevertheless, $LaFe_{0.475}Co_{0.475}Pd_{0.05}O_3$ was found to produce slightly more N_2O (35 ppm) between 160 °C and 240 °C, in comparison to $LaFe_{0.65}Co_{0.3}Pd_{0.05}O_3$. Interestingly the latter catalyst reduced less NO_x compared to $LaFe_{0.475}Co_{0.475}Pd_{0.05}O_3$ suggesting that either Co or Co-species can promote the development of active sites, which participate in the NO_x reduction. Additionally, with respect to the bimetallic particles (i.e., Co and Pd), they may be involved in NO-dissociation and chemisorption, N_2O formation, and H_2-chemisorption. The authors also examined the effect of CO_2 and H_2O given that they are always involved in the exhausts of any combustion engine and can affect the catalyst performance during the H_2-SCR of NO_x reaction. Results from the second series of these catalytic tests showed that the NO conversion dropped when the Co amount in the structure of the perovskite decreased, whereas N_2 selectivity remained constant. When the temperature was lower than 250 °C the NO_x reduction performance decreased, while above 250 °C the NO_x conversion was maintained. Competitive adsorption of H_2O and NO molecules on the active sites of the perovskite was observed, affecting the NO_x conversion, and increasing the formation of N_2O. In addition, as the temperature increased above 250 °C lower amounts of N_2O were produced over the $LaFe_{0.65}Co_{0.3}Pd_{0.05}O_3$ sample [67]. The results from the experiments involving CO_2 and H_2O in the feed gas indicated that H_2O molecules can easily dissociate at increased temperatures on the catalyst surface, facilitating the formation of adsorbed H species, which may eventually lead to higher concentrations of N adsorbed species via the reaction $NO_{ads} + H_{ads} \rightarrow N_{ads} + OH_{ads}$ as also proposed by Dhainaut et al. [83] upon studding the H_2-SCR of NO_x on $Pd/LaCoO_3$ catalysts. Resultantly, more molecular N_2 was formed due to the reaction between two neighboring chemisorbed N atoms on the surface of the $LaFe_{0.65}Co_{0.3}Pd_{0.05}O_3$. The reason why these reactions occurred on catalyst Pd, Pd-Fe, or/and Pd-Co-surface was that the Pd-free sample exhibited no activity for the H_2-SCR of NO_x reaction. Agreeing with Dhainaut et al. [83], the authors stated that the physicochemical properties of Pd were strongly affected by its interaction with La [67]. On the other hand, the $LaFe_{0.475}Co_{0.475}Pd_{0.05}O_3$ catalyst displayed improved NO_x conversion in the presence of H_2O vapor in the feed. Results suggested that 20% more NO_x was reduced for the H_2O-containing mixture in comparison to that or H_2O-free mixture (dry conditions) at 350 °C [67]. Decreased amount of N_2O was also observed with H_2O vapor in the reaction that took place below 250 °C, while at higher temperatures N_2O formation was almost constant. Under these conditions, H_2O was more likely to be dissociated on the $LaFe_{0.475}Co_{0.475}Pd_{0.05}O_3$ surface promoting the formation of molecular N_2 and lowering the chance of N_2O formation. The authors suggested that the improved N_2 selectivity of Pd-La perovskites was probably assigned to the existence of alloy compounds (e.g., Pd_3La) as was also reported by others [66,84]. The effect of CO in the feed was also examined in the third experimental protocol and it was found that both the N_2 selectivity and the NO_x conversion for $LaFe_{0.475}Co_{0.475}Pd_{0.05}O_3$ and $LaFe_{0.65}Co_{0.3}Pd_{0.05}O_3$ perovskites were negatively affected by CO presence [67]. $LaFe_{0.475}Co_{0.475}Pd_{0.05}O_3$ exhibited higher N_2 selectivity compared to that of $LaFe_{0.65}Co_{0.3}Pd_{0.05}O_3$ reaching 54% at 180 °C and 46% as the temperature ranged from 210 to 290 °C. Increasing the Fe-content led to decreased NO_x reduction performance for temperatures above 225 °C. Regarding the $LaFe_{0.65}Co_{0.3}Pd_{0.05}O_3$ catalyst, lower N_2-formation rates were observed while the maximum value of N_2 selectivity was 34% at 237 °C. A 10% decrease was noticed at higher temperatures (i.e., 340 °C) because of the relatively high N_2O concentration formed. Results suggested that higher Co-content in the catalyst, resulted in the formation of perovskite phase, as corroborated by in situ

XRD measurements. Another conclusion made was that the new intermetallic phases, which can be formed between the metallic Fe, Pd, and Co perovskite components, were more resistant to CO poisoning.

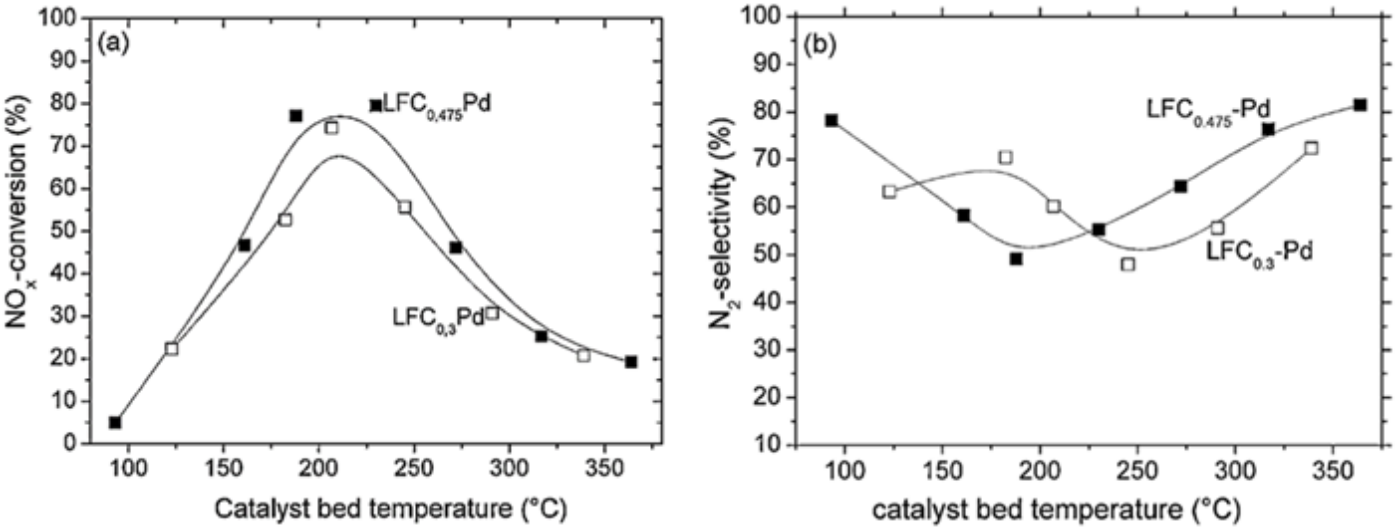

Figure 11. NO_x conversion (**a**) and N_2-selectivity (**b**) of $LaFe_{0.475}Co_{0.475}Pd_{0.05}O_3$ and $LaFe_{0.65}Co_{0.3}Pd_{0.05}O_3$ perovskite catalysts. The samples were calcined at 900 °C in air for 3 h. Reproduced with permission from Ref. [67]. Copyright 2010, Elsevier.

Mondragon Rodriquez et al. [85] have also prepared, via a co-precipitation method, two different perovskite-based catalysts, namely $BaTi_{0.95}Pd_{0.05}O_3$ and $Pd/BaTiO_3$, to evaluate their catalytic performance in the H_2-SCR of NO_x reaction. Four experimental protocols were adopted in the study to decipher the effects of H_2O, CO_2, and CO co-feed, the WGHSV employed, as well as the calcination temperature of the materials during preparation. H_2-TPR, XPS, SEM, TEM, and XRD measurements were adopted for the characterization of the materials under consideration. A TEM image of the $BaTi_{0.95}Pd_{0.05}O_3$ perovskite calcined at 700 °C is shown in Figure 12a. Interestingly, a low Pd-content was found by the EDX-point measurements in the matrix (Figure 12a, arrow), while from Figure 12b qualitatively noticeable Pd-peaks were detected at various sites of the material. EF-TEM analysis was also applied to elucidate the presence of Pd particles before and after reduction pretreatment (Figures 12a and 13b). That said, images using exclusively electrons of a specific energy loss were tracked via an imaging filter. In particular, Figure 13b showed the elemental distribution of Pd, which was calcined in air. Even though the reduction pretreatment was postponed in this sample, many Pd-containing particles were detected in the mapped image. On the other hand, from Figure 13a these particles were hardly visible, while their chemical nature was hardly identified. It was also reported that both Pd-containing perovskite phases and Pd-oxides may be present. Following exposure to the electron beam during the reduction of PdO metallic Pd can also be formed. Besides this vagueness, it was obvious that Pd-rich nanoparticles were present in the catalyst. The catalytic results showed that the use of a high calcination temperature deteriorates the $deNO_x$ activity of the $BaTi_{0.95}Pd_{0.05}O_3$ perovskite: the calcined at 500 °C $BaTi_{0.95}Pd_{0.05}O_3$ catalyst exhibited higher NO conversion (ca. 90%) than that calcined at 900 °C, due to the lower surface area (53% lower) of the latter [85]. However, with respect to the N_2 selectivity, no significant effects resulted. Under the use of a very high WGHSV ($1.61 \cdot 10^6$ $mL \cdot g^{-1} \cdot h^{-1}$), the authors reported maximum NO conversions of 50% at 250 °C and 70% at 200 °C for $BaTi_{0.95}Pd_{0.05}O_3$ and $Pd/BaTiO_3$ catalysts, respectively (Table 2). Considering the high space velocity of these catalytic tests, NO_x conversions were decent. In general, $Pd/BaTiO_3$catalyst outperformed the $BaTi_{0.95}Pd_{0.05}O_3$ catalyst in terms of catalytic activity below 250 °C, though more N_2O was formed (Figure 14). On the other hand, above 250 °C

the $BaTi_{0.95}Pd_{0.05}O_3$ sample exhibited higher NO_x conversion compared to the $Pd/BaTiO_3$ catalyst. It was also found [85] that the addition of CO in the feed afflicted the NO_x conversion, particularly in the temperature range of 160–195 °C. The authors argued that the negative effect of the presence of CO was smaller in comparison to the results presented in the literature. They also highlighted the oxidation potential of Pd which can promote the chemical adsorption of CO on Pd-containing surfaces below 200 °C. However, below this temperature, CO adsorption probably competed with NO_x reduction for occupying the same active sites. Above 200 °C, higher rates of CO oxidation were observed, though they still blocked the active sites of the catalyst compromising the NO_x reduction process. On this basis, small NO_x reduction levels were achieved in the presence of CO, while increased N_2O formation rates were found between 160 and 195 °C. Finally, the conversion of NO_x was further decreased upon increasing the temperature while with respect to N_2 selectivity a medium fluctuation was reported. The appearance of two maxima of the NO_x conversion obtained between 150 and 200 °C during the NO_x reduction in the presence of CO was not interpretable from the available data. In the presence of CO_2 and H_2O, the catalyst maintained 58.7% of NO_x conversion for temperatures between 160 and 195 °C. Above 230 °C, maximum NO_x conversion (ca. 71.5%) was recorded, however, a further increase led to an inverse correlation between temperature and conversion. A beneficial effect on the catalytic performance of $BaTi_{0.95}Pd_{0.05}O_3/900$ (calcined at 900 °C) was reported for temperatures between 195 and 270 °C, suggesting slightly decreased N_2O formation in this temperature range. A positive effect by the addition of CO_2 and H_2O on NO conversion was also found for the $BaTi_{0.95}Pd_{0.05}O_3/900$ catalyst. Nevertheless, below 200 °C, the presence of H_2O resulted in a complex mechanism with antagonistic reactions, (i.e., N_2O and N_2 formation versus NO_x reduction), however above 200 °C the conversion of NO_x was improved. This behavior was attributed to the co-adsorption of CO_2 and H_2O during the NO_x reduction. Moreover, above this temperature H_2O dissociation and H_2O adsorption may be involved in the NO_x reduction mechanism [85].

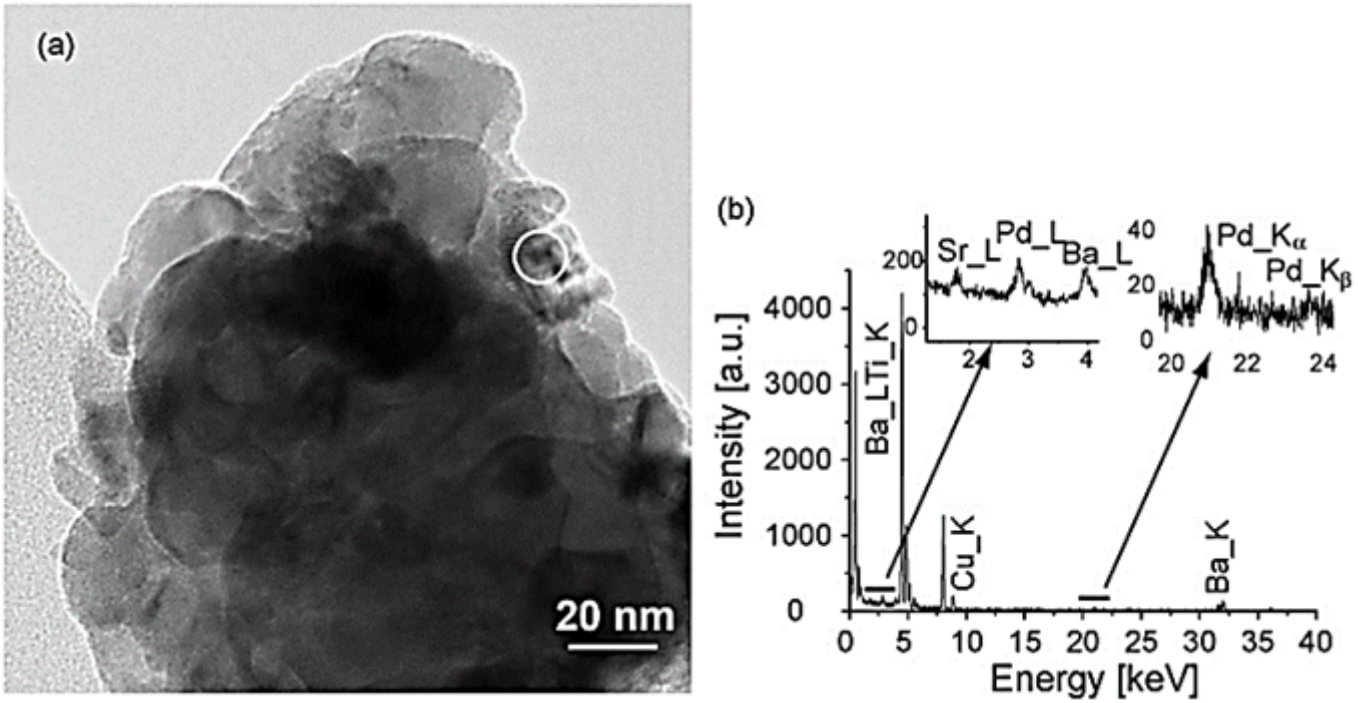

Figure 12. TEM of the $BaTi_{0.9}5Pd_{0.05}O_3$ calcined up to 700 °C/3 h (in air): (**a**) a minute part of an agglomerate, (**b**) EDS spectrum of matrix area encircled in image a, regions containing the Pd–K and Pd–L X-ray diffractions are scaled up to provide a visible Pd-signal. Reproduced with permission from Ref. [85]. Copyright 2010, Elsevier.

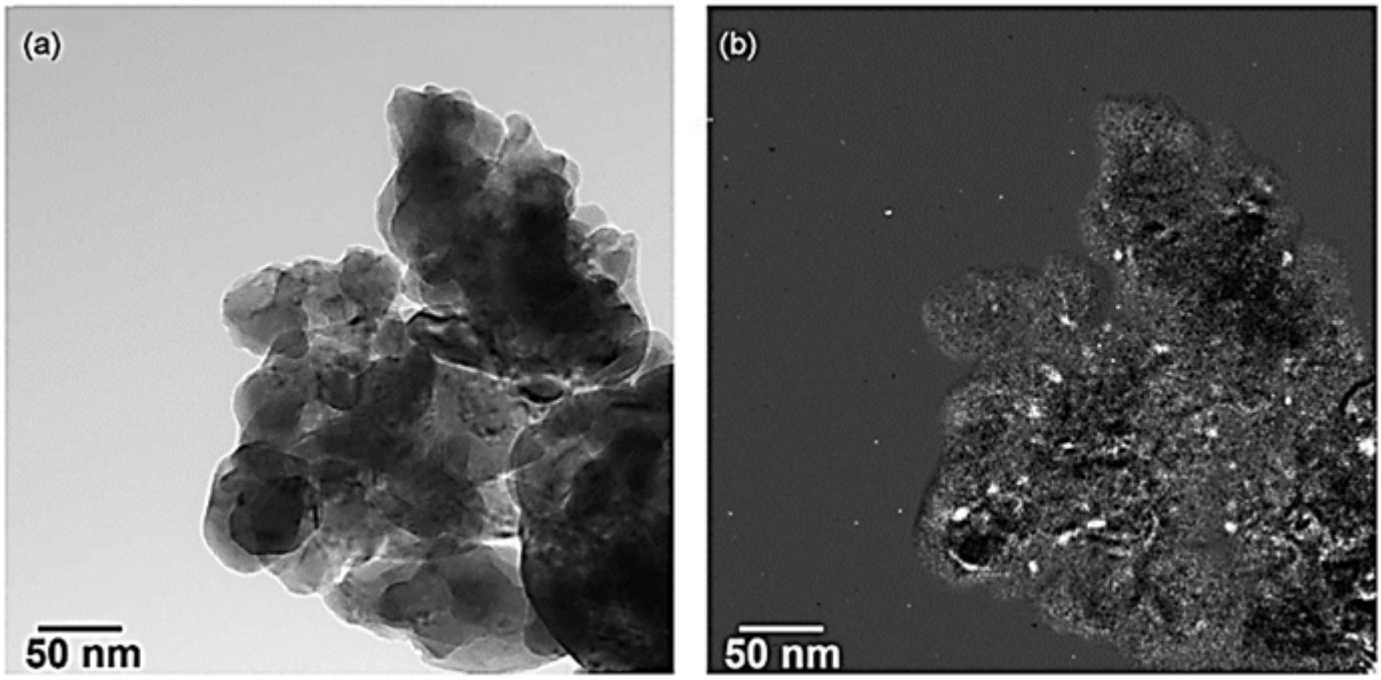

Figure 13. TEM of $BaTi_{0.95}Pd_{0.05}O_3$ calcined up to 700 °C/3 h (in air), (**a**) image of a zero-loss filtered bright field (10 eV slit width), and (**b**) image of Pd elemental map using the 3-window method (i.e., 60 s/window, 20 eV slit width, slit centered at 315 eV, 325 eV, and 410 eV). Reproduced with permission from Ref. [85]. Copyright 2010, Elsevier.

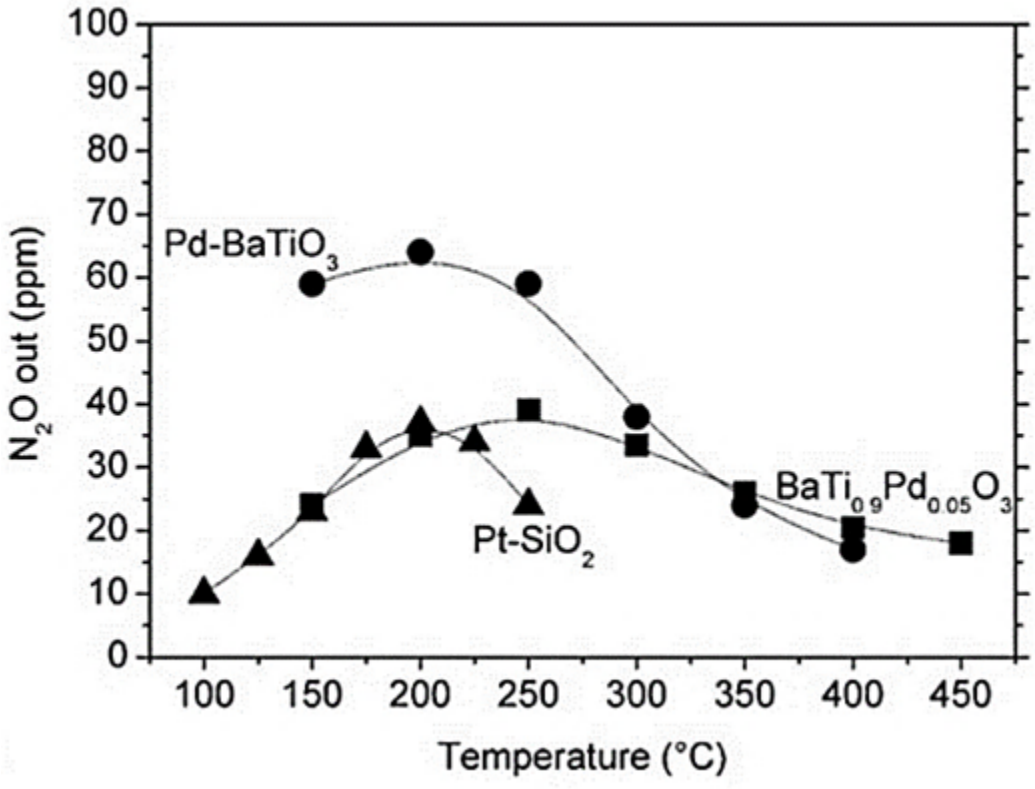

Figure 14. N_2O formation of the catalysts (i.e., Pd-$BaTiO_3$, Pt-SiO_2, $BaTi_{0.95}Pd_{0.05}O_3$). Reproduced with permission from Ref. [85]. Copyright 2010, Elsevier.

In order to highlight the benefits that can be achieved for the H_2-SCR of NO_x using perovskite-type catalysts, i.e., perovskites and/or perovskites promoted by very low noble metal (NM) loadings, in Table 2 we present comparative representative results obtained

using perovskite-based catalysts and conventional supported noble metal catalysts. It can be concluded that perovskite-based catalysts are highly active and significantly selective toward N_2 at temperatures typically below 200 °C; the achievements on these catalysts are well compared to those obtained using the more expensive NM-based conventional catalysts, typically containing higher NM loadings.

Table 2. Comparative presentation of the achievements obtained for H_2-SCR of NO_x by using representative perovskite-based catalysts and conventional-type noble metal catalysts.

Catalyst	Reaction Feed Conditions					Achievements			Ref.
	NO (%)	H_2 (%)	O_2 (%)	Other (%)	WGHSV ($mL \cdot g^{-1} \cdot h^{-1}$)	X_{NO} (%)	at T (°C)	max. S_{N2} (%)	
Perovskite and NM/perovskite catalysts									
$LaFe_{0.65}Co_{0.3}Pd_{0.05}O_3$	0.072	1	5	7.2 (H_2O) + 7.2 (CO_2)	55,400	>50 (max. 57)	200–250	75 (at 200 °C)	[67]
$LaFe_{0.475}Co_{0.475}Pd_{0.05}O_3$	0.072	1	5	7.2 (H_2O) + 7.2 (CO_2)	55,400	>50 (max. 85)	175–300	76 (at 250 °C)	[67]
$La_{0.8}Sr_{0.2}Fe_{0.9}Pd_{0.1}O_3$	0.1	1	5	-	180,000	>50 (max. 96)	120–210	67 (at 160 °C)	[81]
$BaTi_{0.95}Pd_{0.05}O_3$	0.072	1	5	7.2 (H_2O) + 7.2 (CO_2)	55,400	>50 (max. 92)	150–300	72 (at 200 °C)	[85]
$BaTi_{0.95}Pd_{0.05}O_3$	0.045	0.8	5	-	$1.61 \cdot 10^6$	>50 (max. 55)	200–300	68 (at 250 °C)	[85]
$Pd/BaTiO_3$	0.045	0.8	5	-	$1.61 \cdot 10^6$	>50 (max. 70)	125–250	60 (at 150 °C)	[85]
$0.3\%Pt/La_{0.7}Sr_{0.2}Ce_{0.1}FeO_3$	0.25	1	5	-	40,000	>50 (max. 83)	125–225	93 (at 170 °C)	[9]
$0.1\%Pt/La_{0.5}Ce_{0.5}MnO_3$	0.25	1	5	5(H_2O)	40,000	>50 (max. 88)	125–175	78 (at 150 °C)	[86]
Conventional, supported on oxide supports, NM catalysts									
$1\%Pt/SiO_2$	0.072	1	5	7.2 (H_2O) + 7.2 (CO_2)	55,400	>50 (max. 80)	100–175	51 (at 125 °C)	[67]
$1\%Pt/Al_2O_3$	0.05	0.2	6	-	120,000	50	150	30	[82]
$1\%Pt/SiO_2$	0.05	0.2	6	-	120,000	>50 (max. 76)	85–110	20	[82]
$0.5\%Pt/Al_2O_3$	0.05	0.4	5	-	120,000	>50 (max. 80)	100–225	60 (at 175 °C)	[87]
$0.5\%Pd/Al_2O_3$	0.05	0.4	5	-	120,000	9	275	72	[87]
$1\%Pd/Al_2O_3$	1	1	1		100,000	30	160	23	[88]
$0.1\%Pt/MgO\text{-}CeO_2$	0.25	1	5	5(H_2O)	40,000	>50 (max. 95)	90–250	78 (at 150 °C)	[65]
$0.5\%Pd/Al_2O_3$	0.1	0.75	6	0.25(CO)	240,000	30	210	70	[89]
$0.5\%Pd/Al_2O_3\text{-}(10\%TiO_2)$	0.1	0.75	6	0.25(CO)	240,000	>50 (max. 92)	160–450	70 (at 265 °C)	[89]

2.3. Perovskite Catalysts in CO-SCR of NO_x

It is worth noting that our literature search on the perovskites-catalyzed selective (i.e., at excess O_2 conditions) reduction of NO_x by CO was virtually fruitless as we managed to unearth only one publication [90]. On the contrary, and to our surprise, many reports were found on the reduction of NO by CO in the absence of O_2. The former unexplained lack of interest can be partly understood by the fact that the management of CO as an externally supplied reducing agent (as is normally followed in the case of NH_3–, HCs–, or H_2–SCR processes) is difficult due to the extremely dangerous nature of this molecule. However, it should be noted that in many practical combustion processes CO is contained in a high concentration in the exhaust gases together with excess O_2 [13,87,89]. Therefore, it would be of great interest to exploit its existence in the exhaust gases to reduce the coexisting NO_x (i.e., CO-SCR of NO_x) regardless of the fact that its external supply is not desirable. In the following lines we first analyze the report that was found to be directly related to the CO-SCR of NO_x (i.e., the presence of excess O_2) on perovskite-based catalysts, and then, due to the importance of the topic, we consciously choose to deviate slightly from the title of the present review by analyzing the literature on reduction of NO by CO over perovskites even in the absence of O_2.

Qin et al. [90] investigated the effect of ceria-content in $La_xCe_{1-x}FeO_3$ (x = 0.2, 0.4, 0.6, 0.8, 1) perovskite catalysts on improving SO_2 resistance for catalytic reduction of NO with CO in the presence of O_2. Specifically, the feed gas was comprised of 400 ppm NO/500 ppm CO/3% O_2/3% H_2O/(100 ppm SO_2) balance N_2 at a GHSV of 24,000 h^{-1}, and the temperature range of catalytic tests was 100–500 °C. The perovskites were characterized by SO_2–TPD, CO–TPR, XRD, and XPS measurements. In the absence of H_2O, O_2, and SO_2 in the feed (NO + CO reaction) results suggested better catalytic performance with respect to both NO conversion (Figure 15a) and N_2– selectivity (Figure 15b) of $LaFeO_3$ catalyst. To investigate the effect of SO_2 in the NO conversion activity of the perovskites 100 ppm of

SO_2 was added into the NO + CO feed after 30 min of operation and the transient experiments were kept running for a total of 300 min time-on-stream (Figure 15c). Obviously, the existence of SO_2 inhibits the catalytic activity of all perovskites but to a different degree. $La_{0.6}Ce_{0.4}FeO_3$ was less inhibited in the presence of SO_2 highlighting the beneficial effect of substituting La by Ce in the A-sites of the perovskite on its resistance to SO_2-poisoning. It is also apparent that exceeding La substitution by Ce in the perovskite is detrimental to both activity (Figure 14a) and SO_2-poisoning resistance (Figure 15c). The authors also evaluated the materials at CO-SCR conditions, i.e., in the presence of excess O_2, and co-presence of H_2O, and SO_2 (Figure 15d). The $La_{0.6}Ce_{0.4}FeO_3$ perovskite which was found to be optimal in the previous sets of experiments was again optimal in this case in particular at high temperature, however, no results for nitrogen-containing products are available in order to see its N_2-selectivity behavior as well; actually, at high temperatures, the NO_2 production via the NO + O_2 reaction is favored. Based on their characterization results, the authors conclude that the optimal $La_{0.6}Ce_{0.4}FeO_3$ catalyst retains its original structure during the reaction, and the specific redox properties of Ce in its structure are the cause of its superior activity and SO_2 tolerance performance [90].

We now turn our attention to works that report on the performance of perovskite materials during the reduction of NO by CO in the absence of O_2. Wu et al. [91] employed a sol–gel method to prepare $LaM_{0.5}Mn_{0.5}O_3$ (M = Cu, Co, Fe, Ni, Cr) perovskite catalysts in order to evaluate the effect of partial substitution on B-site of this series of catalysts in NO reduction by CO in the absence of O_2 but using excess H_2O (10%) in the feed: 10% CO/5% NO/He balance (i.e., excess CO) and occasionally 10% H_2O and 1000 ppm SO_2. A variety of WGHSVs ranging from 60,000 to 600,000 $mL \cdot g^{-1} \cdot h^{-1}$ were employed, and 72 h time-on-stream stability tests at 250 °C were also conducted. The study includes materials characterization by XPS, ICP-AES, O_2-TPD, H_2-TPR, XRD, BET, and in situ DRIFTS measurements. It was demonstrated that the NO reduction performance of the perovskites clearly improved via the partial substitution of the B-sites by the aforementioned elements, following the order $LaCu_{0.5}Mn_{0.5}O_3$ > $LaCr_{0.5}Mn_{0.5}O_3$ > $LaNi_{0.5}Mn_{0.5}O_3$ > $LaCo_{0.5}Mn_{0.5}O_3$ ≈ $LaFe_{0.5}Mn_{0.5}O_3$ > $LaMnO_3$. $LaCu_{0.5}Mn_{0.5}O_3$ catalyst displayed the best catalytic behavior with complete removal of NO at 300 °C and 100% selectivity toward N_2. On the other hand, the bare $LaMnO_3$ displayed the worst behavior in terms of both NO conversion and N_2-selectivity compared to other Cu-modified perovskites. The authors also examined the stability of the catalysts by carrying out 72-h time-on-stream stability tests at 750 °C. Results indicated that the NO conversion of $LaMnO_3$ dropped from 22.2 to 10.3% whereas the NO conversion of $LaCu_{0.5}Mn_{0.5}O_3$ was barely affected (i.e., 63.8 to 59.3%). The recycle catalytic capacity for 10 cycles was also conducted using the bare $LaMnO_3$ and the optimal $LaCu_{0.5}Mn_{0.5}O_3$ catalysts. A gradual decrease of the catalytic performance was reported for both catalysts, however, the degree of degradation was less significant for the Cu-containing catalyst, highlighting once again the positive role of Cu addition. XRD supportive measurements during these experiments also corroborated the superiority of $LaCu_{0.5}Mn_{0.5}O_3$ over $LaMnO_3$, by showing that the crystallinity of $LaCu_{0.5}Mn_{0.5}O_3$ was less affected (i.e., Cu addition hindered the decrease of crystallinity in the bulk phase) in comparison to that of the bulk phase during the cycles. Moreover, XPS analysis illustrated the existence of constant electron binding energy for the Cu-containing sample during the cycles, indicating an invariant valence state of Mn and La species under the reaction conditions [91]. On the other hand, it was also clear that the $LaMnO_3$ sample was less resistant to the reaction atmosphere. The effect of WGHSV (i.e., 60,000–600,000 $mL \cdot g^{-1} \cdot h^{-1}$) was also studied for these two catalysts showing a gradual shift of the NO conversion profiles to higher temperatures upon increasing space velocity for both catalysts.

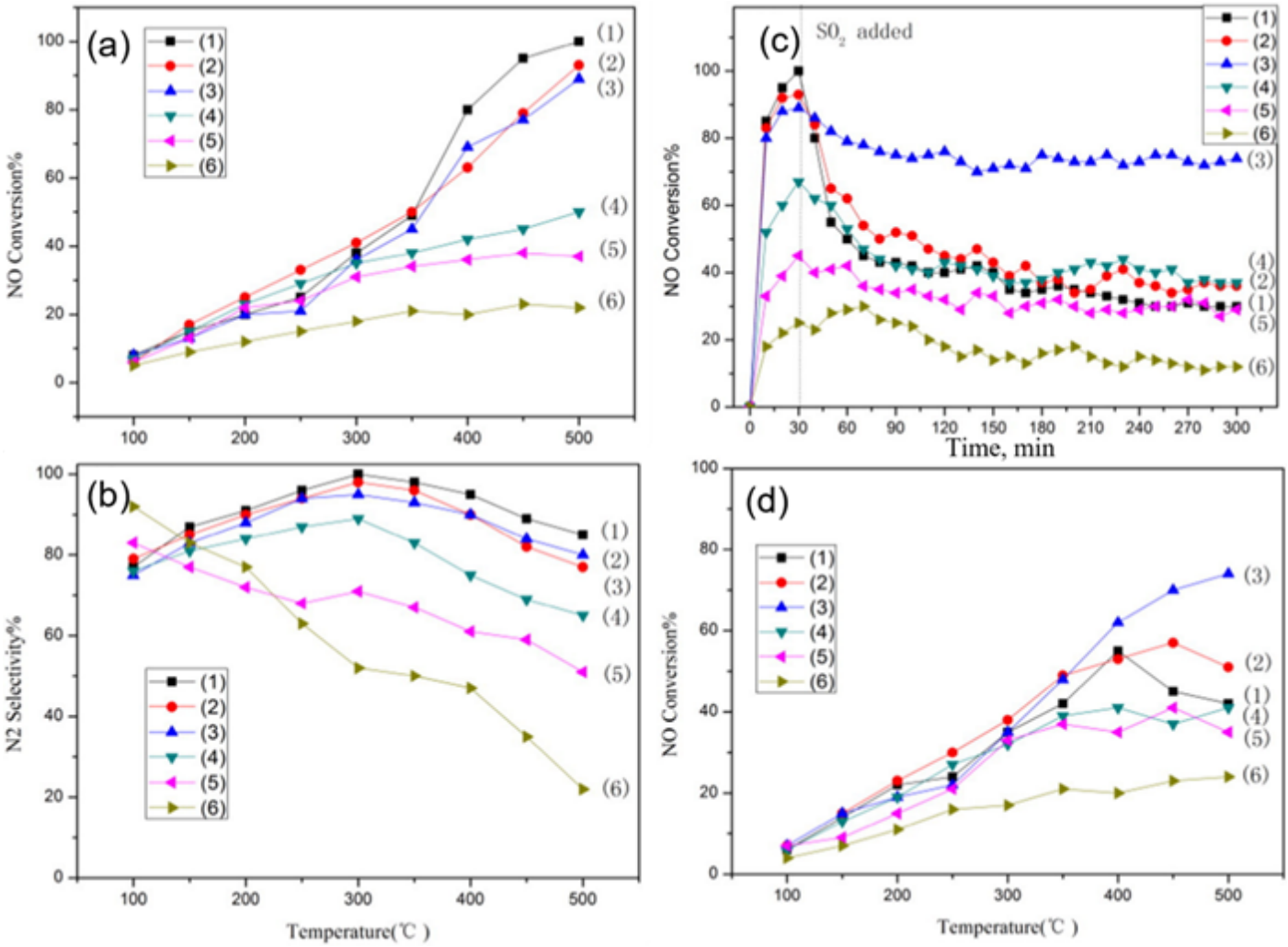

Figure 15. NO conversion over $La_xCe_{1-x}FeO_3$ perovskites during the NO reduction by CO: NO conversion versus temperature from 100 to 500 °C (**a**), and corresponding N_2-selectivities (**b**) using 400 ppm NO/500 ppm CO/He balance at 1 bar and GHSV of 24,000 h^{-1}; NO conversion versus time of $La_xCe_{1-x}FeO_3$ catalysts at 500 °C with 100 ppm SO_2 in the feed (**c**); NO conversion versus temperature of $La_xCe_{1-x}FeO_3$ catalysts in CO + NO reaction with the addition of 100 ppm SO_2, 3% O_2 and 3 vol.% H_2O in the feed (**d**). (1): $LaFeO_3$, (2): $La_{0.8}Ce_{0.2}FeO_3$, (3): $La_{0.6}Ce_{0.4}FeO_3$, (4): $La_{0.4}Ce_{0.6}FeO_3$, (5): $La_{0.2}Ce_{0.8}FeO_3$, and (6): CeO_2. Reproduced with permission from Ref. [90]. Copyright 2016, Elsevier.

The sulfur and H_2O resistance capacity of the optimal $LaCu_{0.5}Mn_{0.5}O_3$ catalyst was also probed during time-on-stream experiments at a constant temperature in which 10% H_2O or 1000 ppm SO_2 or even 10% H_2O + 1000 ppm SO_2 was co-fed with the flowing NO + CO gas mixture (Figure 16) [91]. As can be seen, the addition of H_2O led to an about 16% drop in NO conversion which then maintained approximately constant. When H_2O was removed from the feed, the catalytic performance was only partially restored. The effects of inhibition/recovery on catalytic behavior due to the introduction/removal of SO_2 into the feed stream were qualitatively similar to those of H_2O but more pronounced, and become even more intense when both SO_2 and H_2O are fed (Figure 16). An increase of the temperature from 300 to 400 °C was needed to lead to a complete restoration of catalytic activity after removal of the inhibitors from the feed stream, regardless of their identity. That said, this Cu-containing perovskite catalyst could be considered a fairly good sulfur and H_2O resistant material. In situ DRIFTS experiments enabled the authors to suggest an Eley–Rideal reaction mechanism (Figure 17) which adequately describes their findings. As shown in Figure 17, introducing NO and CO at ambient temperature can lead to the attachment of NO molecules onto the perovskite, covering the active sites indicated in the

figure. Therefore, some nitrates and nitrate-like species may be formed on the perovskite's surface inhibiting the adsorption of CO molecules. Below 200 °C, the adsorbed NO species may react with CO to form N_2, N_2O, and CO_2, as corroborated by both in situ DRIFTS measurements and catalytic runs under a real reaction atmosphere. Above 200 °C, the desorption, dissociation, and conversion of NO species can be observed to form N_2O and N_2 (i.e., NO → [N] + [O], NO + [N] → N_2O, [N] + [N] → N_2).

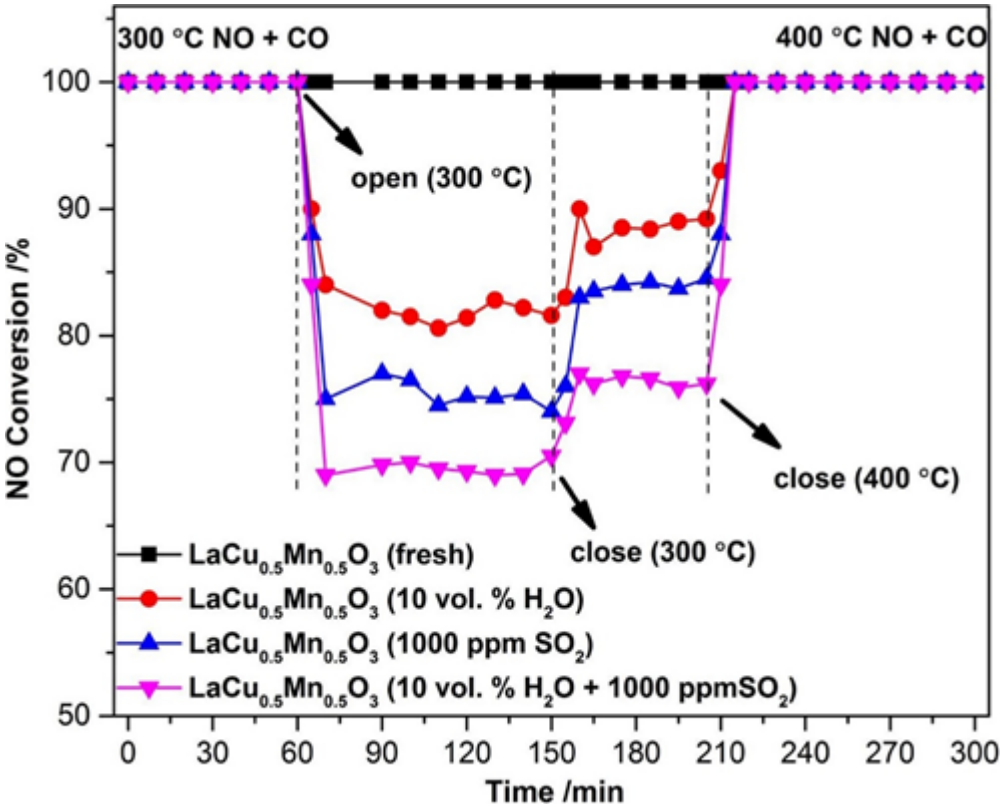

Figure 16. The NO conversions over $LaCu_{0.5}Mn_{0.5}O_3$ catalyst upon adding different reaction inhibiting substances (10% H_2O/1000 ppm SO_2 and 10 % H_2O + 1000 ppm SO_2) in the NO + CO reactor feed stream. Reproduced with permission from Ref. [91]. Copyright 2020, Elsevier.

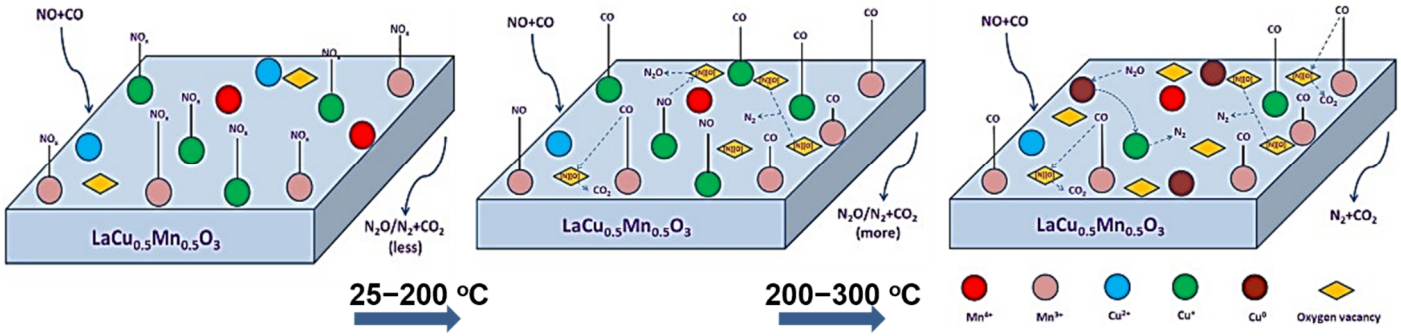

Figure 17. The mechanism of catalytic reduction NO by CO on $LaCu_{0.5}Mn_{0.5}O_3$ perovskites. Reproduced with permission from Ref. [91]. Copyright 2020, Elsevier.

In a different study, using the same preparation method (sol–gel) the research group also prepared a $LaCu_{0.25}Co_{0.75}O_3$ (LCC) perovskite to study the effect of calcination temperature (250, 500, 750, and 1000 °C) on its catalytic performance for NO + CO reaction tested in a feed composition of 10% CO/5% NO/Ar balance at WGHSV = 60,000 $mL \cdot g^{-1} \cdot h^{-1}$ and temperature range between 100–600 °C [92]. Regarding the NO and CO conversion efficiency, the LCC-750 > LCC-500 > LCC-250 > LCC-1000 sequence was found, with

the outperformed LCC-750 sample to achieve complete NO and 50% CO conversions at ~350 °C, and 100% selectivity toward N_2 at ~400 °C. The authors concluded that the ratio of $Cu^+/(Cu^+ + Cu^{2+})$ and $Co^{2+}/(Co^{2+} + Co^{3+})$, the reducibility, and amount of oxygen deficiencies were the key points for the enhancement catalytic behavior observed. Indeed, maximum values of all these ratios and properties were measured on the outperformed LCR-750 catalyst (Figure 18).

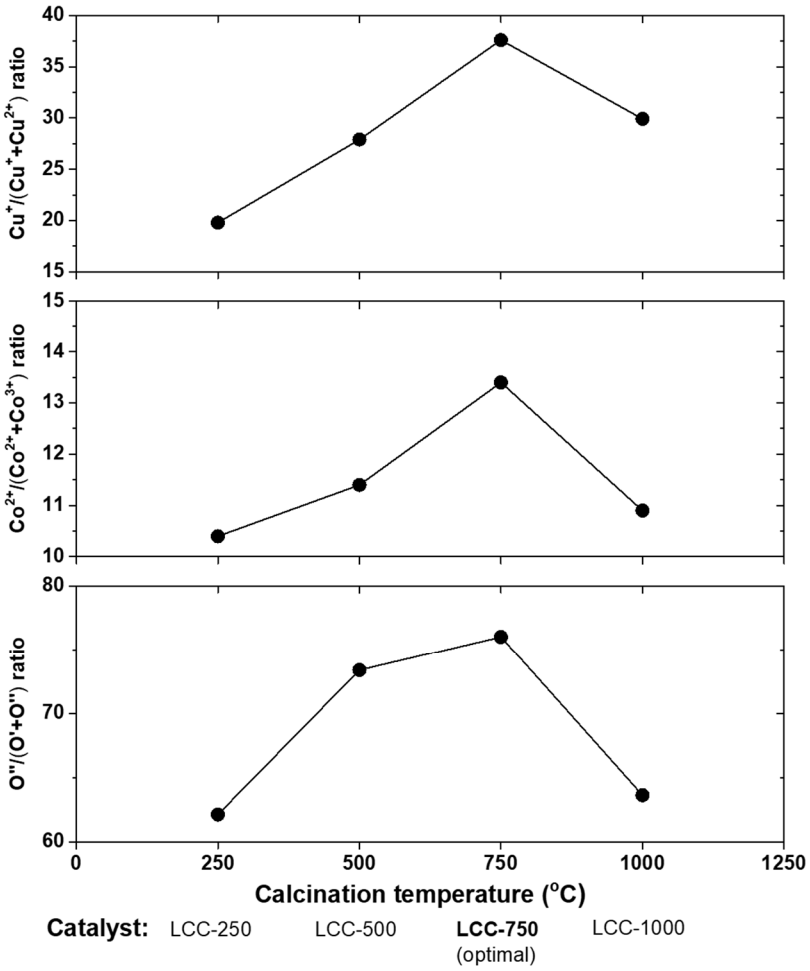

Figure 18. The surface element distribution of LCC-x (x = 250, 500, 750 and 1000 °C) perovskites calcined at different temperatures. O′ and O″ are bulk and chemically absorbed oxygen, respectively; O′ is connected with the redox capacity of the catalysts, and the proportion of O″ is closely linked to the quantity of oxygen deficiency in catalysts. Data were taken with permission from Ref. [92]. Copyright 2019, Elsevier.

In yet another study, the same group reported the effect of B-site partial substitution of a $La_{0.8}Ce_{0.2}M_{0.25}Co_{0.75}O_3$ (M = Fe, Mn, Cu) perovskite on NO reduction by CO [93]. The preparation method and reaction conditions used were similar as above. It was found that the addition of all Fe, Mn, and Cu on the bare $La_{0.8}Ce_{0.2}CoO_3$ perovskite was beneficial to its NO reduction activity, however, the Cu-substituted $La_{0.8}Ce_{0.2}Cu_{0.25}Co_{0.75}O_3$ perovskite outperformed all the other samples on both activity and N_2 selectivity. In terms of maximum achievements, the Cu-substituted perovskite showed 100% NO conversion, 50% CO conversion, and 99% N_2 selectivity at ~300 °C. This catalyst has also been found to be substantially more stable in 48-hours' time-on-stream performance; a slight (82% → 80.3%) compared to a significant (58.8% → 43.6%) degradation of NO conversion activity was recorded for $La_{0.8}Ce_{0.2}Cu_{0.25}Co_{0.75}O_3$ and $La_{0.8}Ce_{0.2}CoO_3$, respectively. The performance

superiority of $La_{0.8}Ce_{0.2}Cu_{0.25}Co_{0.75}O_3$ was attributed to the enhanced amount of O_2 vacancies, texture properties, and reducibility, while the NO + CO reaction kinetics appeared to comply with the Eley–Rideal mechanism [93].

Moreover, the same group also studied a series of $LaNi_{0.5}M_{0.5}O_3$ (M = Co, Mn, Cu) perovskites using again a NO + CO feed with excess CO (i.e., 5% NO/10% CO/85% He at WGHSV = 36,000 $mL \cdot g^{-1} \cdot h^{-1}$) [94]. Results illustrated that the partial (50 mol%) substitution of Ni with Co, Mn, or Cu in $LaNiO_3$ had in all cases a positive effect on its catalytic activity, with Cu-substituted $LaNi_{0.5}Cu_{0.5}O_3$ perovskite outperforming all others in N_2 selectivity at temperatures > 250 °C. In situ DRIFTS experiments enabled the authors to propose a Langmuir–Hinshelwood mechanism for the NO reduction by CO on this series of perovskites as schematically shown in Figure 19, exemplified for $LaNi_{0.5}Cu_{0.5}O_3$ perovskite [94]. According to the mechanism, at low temperatures (50–150 °C) NO is preferentially adsorbed on the active sites of the perovskite surface forming nitrates, which can be gradually desorbed and react with gaseous CO forming small amounts of N_2O, N_2, and CO_2. In the temperature region 150–250 °C, Cu^{2+} is reduced to Cu^{+} providing sites for CO chemisorption that produce some carbonate and carboxylate species. At the same time, surface oxygen vacancies can activate NO dissociative adsorption and facilitate N_2O decomposition. The as derived dissociative products can further react with adsorbed CO forming CO_2 and N_2O. For high temperatures (ca. 250 °C and higher) chemisorbed O species began to desorb regenerating oxygen vacancy sites. The increased availability of the latter sites further facilitates NO and N_2O dissociation. Then Cu^{2+} sites can be regenerated via $Ni^{3+} + Cu^{+} \leftrightarrow Ni^{2+} + Cu^{2+}$, and Cu^{+} also can be oxidized by N_2O to Cu^{2+} leading to N_2O conversion toward N_2 (Figure 19) [94].

Tarjomannejad et al. [95] prepared via a sol–gel method $LaMn_{1-x}Fe_xO_3$ (x = 0, 0.3, 0.5, 0.7, 1) and $La_{0.8}M_{0.2}Mn_{0.3}Fe_{0.7}O_3$ (M = Ce, Ba, Cs, Sr) perovskites to evaluate their performance in catalytic reduction of NO by CO under a 3000 ppm NO/3000 ppm CO/Ar balance gas feed at a WGHSV = 12,000 $mL \cdot g^{-1} \cdot h^{-1}$ in the temperature range between 150 and 500 °C. The catalysts under consideration were characterized using SEM, H_2-TPR, XPS, BET, and XRD techniques. Results showed that the $LaMn_{0.3}Fe_{0.7}O_3$ catalyst exhibited the highest catalytic activity when compared to the other catalysts of the $LaMn_{1-x}Fe_xO_3$ group. In particular, the catalytic activity of this group followed the order $LaMnO_3 < LaFeO_3 < LaMn_{0.7}Fe_{0.3}O_3 < LaMn_{0.5}Fe_{0.5}O_3 < LaMn_{0.3}Fe_{0.7}O_3$. It was reported that the partial substitution of Mn by Fe in the perovskite led to the formation of O_2 vacancies promoting the catalyst's reducibility. The introduction of a small amount of Ce, Sr, Cs into the A-site of the perovskite had a beneficial effect on catalytic performance. In contrast, partial substitution of La by Ba compromised the catalyst activity. On this basis the catalytic activity followed the order $La_{0.8}Ba_{0.2}Mn_{0.3}Fe_{0.7}O_3 < LaMn_{0.3}Fe_{0.7}O_3 < La_{0.8}Cs_{0.2}Mn_{0.3}O_3 < La_{0.8}Sr_{0.2}Mn_{0.3}Fe_{0.7}O_3 < La_{0.8}Ce_{0.2}Mn_{0.3}Fe_{0.7}O_3$. The authors concluded that the enhanced activity of the best and second-best catalyst (obtained by substitution of La by Ce^{4+} and Sr^{2+} in the A-site) was due to the induced chances in the reducibility of B-site cations, Mn^{4+}/Mn^{3+}, and Fe^{4+}/Fe^{3+} ratios, and increase the O_{ads}/O_{latt} ratio, factors that increase the number of structural defects in the perovskite structure. In an additional publication of the research group [35], $LaCu_{0.7}B_{0.3}O_3$ (B = Mn, Fe, Co) perovskites were synthesized and comparatively evaluated in NO + CO reaction at feed conditions such as the above. After finding the superiority of $LaCu_{0.7}Mn_{0.3}O_3$, they further modified the A-sites of this perovskite by an alkali or alkaline earth metal (Rb, Sr, Cs, Ba) and concluded that $La_{0.8}Sr_{0.2}Cu_{0.7}Mn_{0.3}O_3$ was the best among all samples tested, offering 100% NO conversion at 375 °C. The same arguments as in the previous study were invoked to explain their findings.

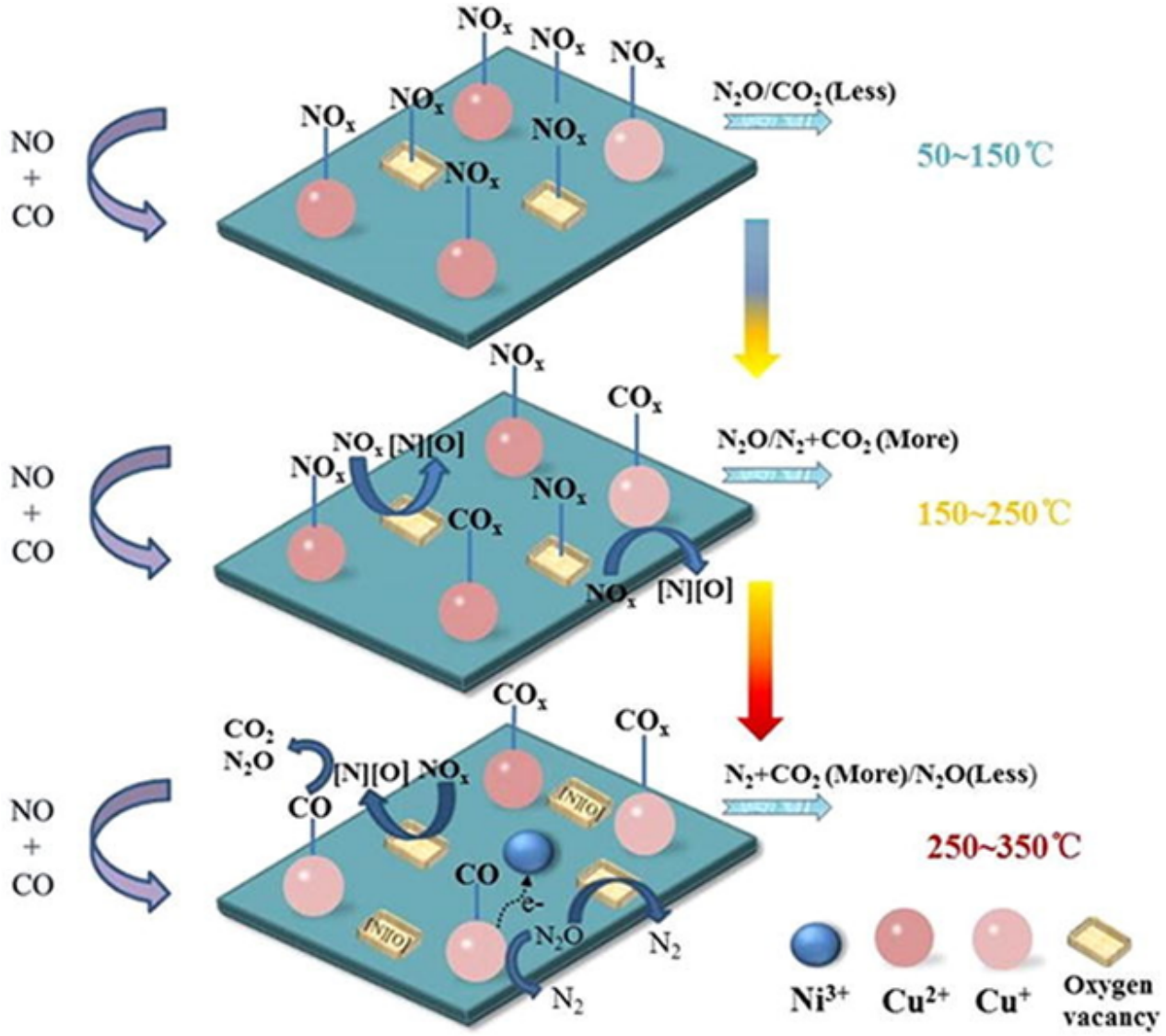

Figure 19. Reaction mechanism for the catalytic reduction of NO by CO on $LaNi_{0.5}Cu_{0.5}O_3$ perovskites. Reproduced with permission from Ref. [94]. Copyright 2019, Elsevier.

The same group [96] prepared two groups of perovskites, $LaFe_{0.5}M_{0.5}O_3$ and $LaMn_{0.5}M_{0.5}O_3$ (M = Cu, Co, Mn, Fe), and evaluated them in NO + CO reaction using stoichiometric conditions (3000 ppm NO/3000 ppm CO/Ar balance at WGHSV = 12,000 $mL \cdot g^{-1} \cdot h^{-1}$ and temperatures between 100 and 450 °C). The catalytic activity for the $LaFe_{0.5}M_{0.5}O_3$ group followed the order LaFeCo < LaFe < LaFeCu < LaFeMn. The catalytic activity for the $LaMn_{0.5}M_{0.5}O_3$ group followed the order LaMn < LaMnCo < LaMnFe < LaMnCu. Among all the samples tested (both series) the optimal behavior overall was that of $LaMn_{0.5}Cu_{0.5}O_3$. It was associated with a synergistic interaction between Mn and Cu, higher reducibility at low temperatures, and an increased number of structural defects. The authors also examined three different mechanisms for the NO reduction by CO. Among them, the Langmuir–Hinshelwood model was found to be more suitable for describing the kinetic data obtained. More specifically, the proposed mechanism is that described by the following reaction steps (R.1)–(R.6), which is similar to that reported for noble metal catalyzed NO + CO reaction [97,98].

$$NO + * \leftrightarrow NO* \quad (R.1)$$

$$CO + * \leftrightarrow CO* \quad (R.2)$$

$$NO^* + * \rightarrow N^* + O^* \quad \text{(R.3)}$$

$$N^* + N^* \rightarrow N_2 + 2^* \quad \text{(R.4)}$$

$$N^* + NO^* \rightarrow N_2O + 2^* \quad \text{(R.5)}$$

$$CO^* + O^* \rightarrow CO_2 + 2^* \quad \text{(R.6)}$$

De Lima et al. [99] prepared $LaFe_{1-x}Co_xO_3$ perovskites, namely $LaFeO_3$ and $LaFe_{0.6}Co_{0.4}O_3$, synthesized either conventionally (by the citrate method) or using a nanocasting method; the latter leads to materials constituted by more than 97 wt% of perovskite phase and by agglomerates smaller than 100 nm constituted by crystallites of about 6 nm (Figure 20). As a result, the nanocast perovskites had about 10 times larger specific surface areas compared to the conventional perovskites (e.g., 49.3 and 30.5 vs. 5.6 and 3.6 m^2/g for the nanocast and conventional $LaFeO_3$ and $LaFe_{0.6}Co_{0.4}O_3$ perovskites, respectively). These materials were comparatively evaluated in the reduction of NO by CO. Figure 21 shows the results of this comparison. Obviously, the nanocast perovskites are significantly more active than their conventional counterparts, and as the authors conclude this is mainly due to the higher specific surface area of the former and the consequent higher number of accessible active sites exposed to the reactants.

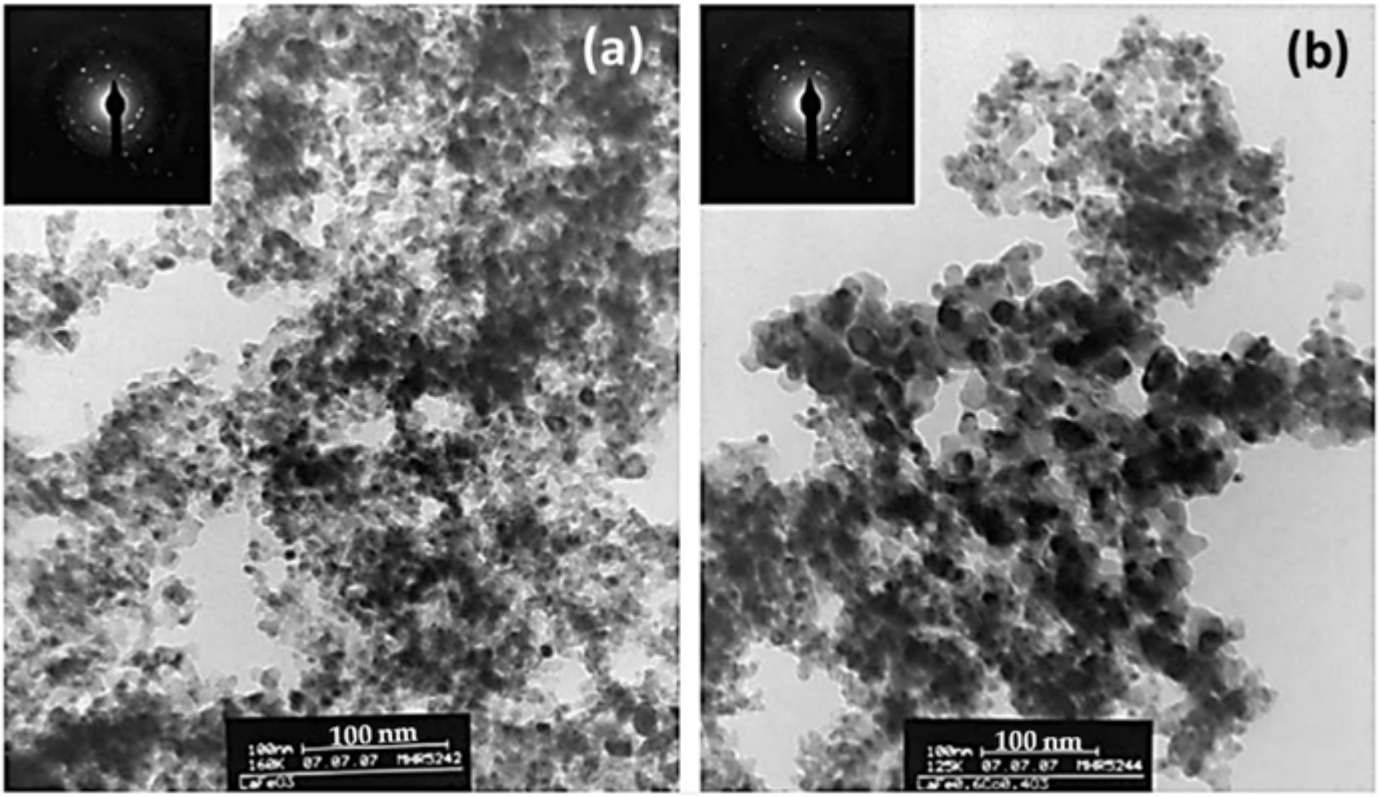

Figure 20. TEM images of $LaFeO_3$ (**a**) and $LaFe_{0.6}Co_{0.4}O_3$ (**b**) prepared by a nanocast method. Reproduced with permission from Ref. [99]**.** Copyright 2009, Elsevier.

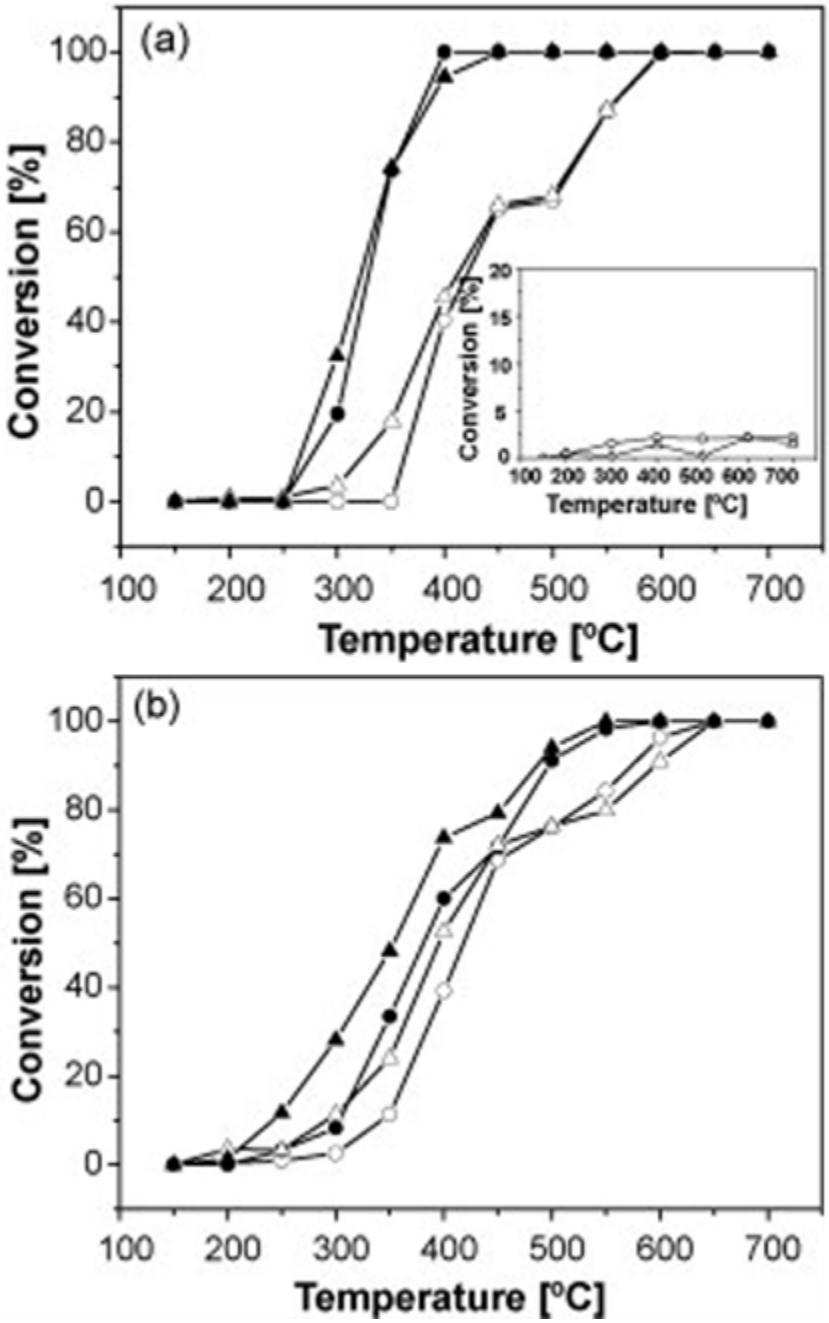

Figure 21. Temperature profiles for the conversion of NO to N_2 (○, ●) and CO to CO_2 (▵ , ▲) on: (a) uncast $LaFeO_3$ (○, ▵) and nanocast $LaFeO_3$ (●, ▲). Inset: conversion of NO to N_2 (○) and CO to CO_2 (▵) without any catalyst; (b) uncast $LaFe_{0.6}Co_{0.4}O_3$ (○, ▵) and nanocast $LaFe_{0.6}Co_{0.4}O_3$ (●, ▲). Reproduced with permission from Ref. [99]. Copyright 2009, Elsevier.

Finally, aiming at three-way catalysis (TWC), Glisenti et al. [59] prepared largely Cu-doped $LaCo_{1-x}Cu_xO_3$ (x = 0, 0.1, 0.3, and 0.5) perovskites by means of the citrate method and tested these materials in model reactions involved in TWC (i.e., NO + CO and CO + O_2) as well as at simulated automotive exhaust conditions. Regarding the NO + CO model reaction the feed gas composition comprised of 4% CO/4% NO/Ar balance at 1 bar with a WGHSV = 150,000 $mL \cdot g^{-1} \cdot h^{-1}$. The catalysts under consideration were characterized by a variety of techniques. XRD results corroborated for a stable perovskite phase holding a rhombohedral geometry with the crystallite size to be decreased upon increasing the copper amount. XPS results suggested that the addition of Cu caused the decrease of Co(III)

→ Co(II) → Co(0) reduction temperatures, as a result of H_2 activation. This H_2 activation can be assigned to the surface segregated Cu clusters and to the increased O_2 mobility because of the formation of vacancies. Regarding the catalytic performance of the materials in NO reduction by CO, it has been shown that the introduction of Cu into the $LaCoO_3$ structure was beneficial as almost complete NO and CO conversions were achieved at 400 °C. Specifically, the catalytic activity of the samples followed the order $LaCoO_3$ < $LaCo_{0.9}Cu_{0.1}O_3$ < $LaCo_{0.7}Cu_{0.3}O_3$ < $LaCo_{0.5}Cu_{0.5}O_3$. That is the perovskite with the highest Cu doping outperformed the other samples (Figure 22); notably, N_2 was the main N-containing reaction product [59].

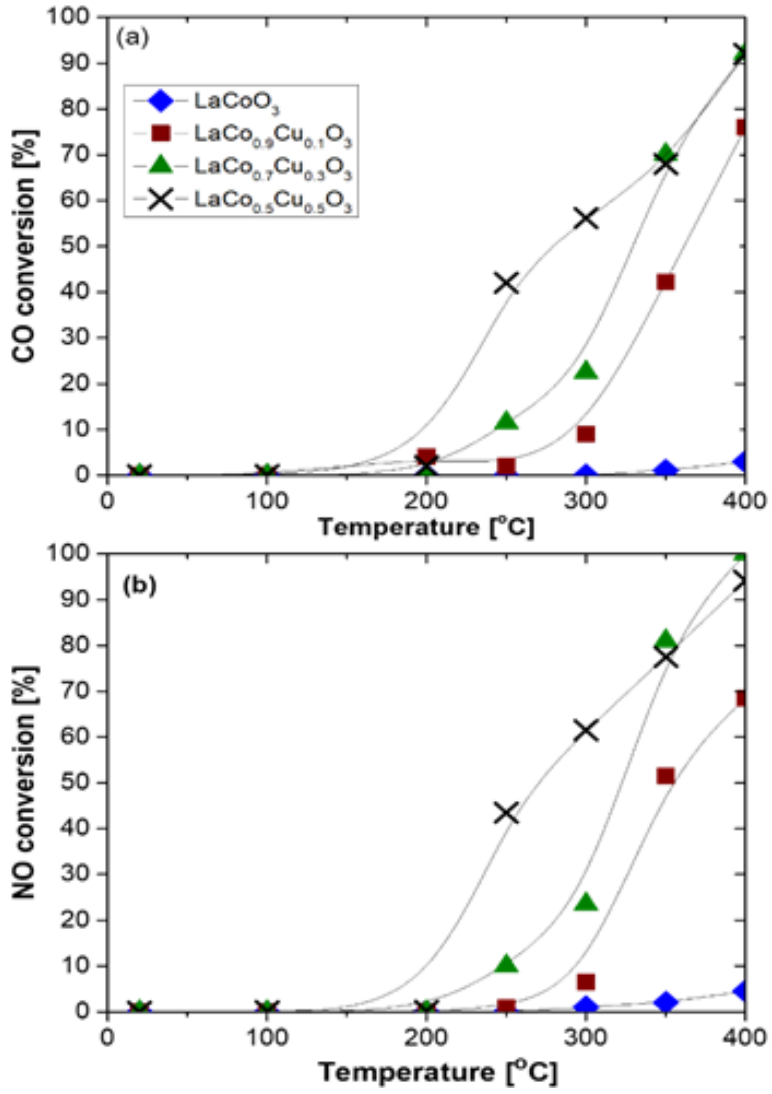

Figure 22. CO (**a**) and NO (**b**) conversion as a function of temperature on $LaCo_{0.5}Cu_{0.5}O_3$, $LaCo_{0.7}Cu_{0.3}O_3$, $LaCo_{0.9}Cu_{0.1}O_3$, and $LaCoO_3$ perovskites. Conditions: 4% NO/4% CO/balance He at 1 bar; WGHSV = 150,000 mL·g^{-1}·h^{-1}. Reproduced with permission from Ref. [59]. Copyright 2016, Elsevier.

As in the previous sections, we constructed Table 3 here, comparing the aforementioned results (and some additional ones) from the literature on NO reduction by CO using perovskite catalysts, even though, as mentioned at the beginning of the section, literature on the selective catalytic reduction (i.e., in excess of O_2) of NO_x by CO is rather rare. For comparison, the table also includes some representative results on the titled reaction catalyzed by NM-based catalysts.

Table 3. Representative literature for NO reduction by CO over perovskites and on transitional noble metal catalysts.

Catalyst	Reaction Conditions					Achievements			Ref.
	NO (%)	CO (%)	O_2 (%)	Other (%)	WGHSV (mL/g·h)	X_{NO} (%)	at T (°C)	max. S_{N2} (%)	
Perovskite catalysts									
$La_{0.6}Ce_{0.4}FeO_3$ [a]	0.04	0.05	-	-	24,000 h^{-1} (GHSV)	>50 (max. 88)	350–500	90 (at 350)	[90]
$La_{0.6}Ce_{0.4}FeO_3$ [a]	0.04	0.05	-	0.01 (SO_2)	24,000 h^{-1} (GHSV)	76	500	n/a	[90]
$La_{0.6}Ce_{0.4}FeO_3$ [a]	0.04	0.05	3	0.01 (SO_2) + 3 (H_2O)	24,000 h^{-1} (GHSV)	>50 (max. 74)	350–500	n/a	[90]
$LaCu_{0.5}Mn_{0.5}O_3$ [b]	5	10	-	-	60,000	100	300–600	100	[91]
$LaCu_{0.25}Co_{0.75}O_3$-750 [c]	5	10	-	-	60,000	100	350–600	100	[92]
$La_{0.8}Ce_{0.2}Cu_{0.25}Co_{0.75}O_3$ [d]	5	10	-	-	60,000	100	290–600	100	[93]
$LaNi_{0.5}Cu_{0.5}O_3$ [e]	5	10	-	-	36,000	100	375–500	100 (at 450 °C)	[94]
$LaMn_{0.3}Fe_{0.7}O_3$ [f]	0.3	0.3	-	-	12,000 h^{-1} (GHSV)	90–100	390–450	90–100	[95]
$La_{0.8}Ce_{0.2}Fe_{0.7}Mn_{0.3}O_3$ [g]	0.3	0.3	-	-	12,000 h^{-1} (GHSV)	90–100	340–450	92–96	[95]
$LaFe_{0.5}Mn_{0.5}O_3$ [h]	0.3	0.3	-	-	12,000 h^{-1} (GHSV)	90–100	420–450	92–96	[96]
$LaMn_{0.5}Cu_{0.5}O_3$ [i]	0.3	0.3	-	-	12,000 h^{-1} (GHSV)	90–100	400–450	90–98	[96]
$LaFeO_3$-nanocast	0.5	0.5	-	-	30,000	100	375–700	100	[99]
$LaFeO_3$-uncast	0.5	0.5	-	-	30,000	100	600–700	100	[99]
$LaFe_{0.6}Co_{0.4}O_3$-nanocast	0.5	0.5	-	-	30,000	100	550–700	100	[99]
$LaFe_{0.6}Co_{0.4}O_3$-uncast	0.5	0.5	-	-	30,000	100	650–700	100	[99]
$LaCo_{0.5}Cu_{0.5}O_3$ [j]	4	4	-	-	150,000	95	400	n/a	[59]
$LaCu_{0.7}Mn_{0.3}O_3$ [k]	0.3	0.3	-	-	12,000 h^{-1} (GHSV)	>90	360–450	n/a	[35]
$La_{0.8}Sr_{0.2}Cu_{0.7}Mn_{0.3}O_3$ [l]	0.3	0.3	-	-	12,000 h^{-1} (GHSV)	>90	320–450	n/a	[35]
$La_{0.8}Ce_{0.2}FeO_3$ [m]	2	2	-	-	30,000	>90	330–500	n/a	[64]
$LaMnO_3$ (r); $LaFeO_3$ (r) *	2	2	-	-	30,000	>90	420–500	n/a	[100]
$LaMnO_3$ [n]	2	2	-	-	30,000	>90	510–570	100	[101]
Conventional, supported on oxide supports, NM catalysts									
0.5wt%Pt/γ-Al_2O_3	0.05	0.4	5	-	120,000	26	250	80	[87]
0.5wt%Pd/γ-Al_2O_3	0.05	0.4	5	-	120,000	13	180	62	[87]
0.5wt%Pt/γ-Al_2O_3	0.1	0.1	-	-	600,000	60	480	60	[102]
0.5wt%Pt(9.7%Rb)/γ-Al_2O_3	0.1	0.1	-	-	600,000	>90	320–500	100 (at 350 °C)	[102]
0.5wt%Rh/γ-Al_2O_3	0.1	0.1	-	-	600,000	>90	250–500	100 (at 300 °C)	[102]

[a] The optimal from a series of $La_xCe_{1-x}FeO_3$ (x = 0.2, 0.4, 0.6, 0.8, 1) perovskites investigated. [b] The optimal from a series of $LaM_{0.5}Mn_{0.5}O_3$ (M = Cu, Co, Fe, Ni, Cr) perovskites investigated. [c] The optimal from a $LaCu_{0.25}Co_{0.75}O_3$ perovskite calcined at differed temperatures (250, 500, 750, and 1000 °C). [d] The optimal from a series of B-site partially substituted $La_{0.8}Ce_{0.2}M_{0.25}Co_{0.75}O_3$ (M = Fe, Mn, Cu) perovskite. [e] The optimal from a series of $LaNi_{0.5}M_{0.5}O_3$ (M = Co, Mn, Cu) perovskites investigated. [f] The optimal from a series of $LaMn_{1-x}Fe_xO_3$ (x = 0, 0.3, 0.5, 0.7, 1) perovskites investigated. [g] The optimal from a series of $La_{0.8}M_{0.2}Mn_{0.3}Fe_{0.7}O_3$ (M = Ce, Ba, Cs, Sr) perovskites investigated. [h] The optimal from a series of $LaFe_{0.5}M_{0.5}O_3$ (M = Cu, Co, Mn, Fe) perovskites investigated. [i] The optimal from a series of $LaMn_{0.5}M_{0.5}O_3$ (M = Cu, Co, Mn, Fe) perovskites investigated. [j] The optimal from a series of $LaCo_{1-x}Cu_xO_3$ (x = 0, 0.1, 0.3, and 0.5) perovskites investigated. [k] The optimal from a series of $LaCu_{0.7}B_{0.3}O_3$ (B = Mn, Fe, Co) perovskites investigated. [l] The optimal from a series of $La_{0.8}A_{0.2}Cu_{0.7}Mn_{0.3}O_3$ (A = Rb, Sr, Cs, Ba) perovskites investigated. [m] The optimal from a series of $La_xM_{1-x}FeO_3$ (M = Sr and/or Ce) perovskites investigated. * Materials prepared by a microemulsion method in the reverse (r) state. [n] The optimal from a series of $La_xSr_{1-x}MnO_3$ perovskites investigated.

3. General Outcomes and Future Perspectives

This work reviews the literature that concerns the use of perovskites and perovskites-based catalysts in the selective catalytic reduction (SCR) of NO_x with different than the typically used NH_3 or urea reducing agents, i.e., C_xH_y/$C_xH_yO_z$, H_2, and CO. The main purpose of this undertaking is to present the state-of-the-art in the field, which could help industry and academia become aware of new possibilities and perspectives in order to meet future requirements in addressing NO_x emissions.

The urgency of developing efficient approaches for NO_x emission control in order to meet increasingly stringent environmental requirements is widely accepted. Significant downsides are associated with low NO_x concentration and excess oxygen in the exhaust gas, conditions under which the competitive role of dioxygen in the oxidation of reducing agents to the detriment of NO_x reducing reactions to harmless N_2 is major. During SCR of

NO_x, several catalysts and conditions can also favor N_2O production which has undesirable high global warming potential and is also the main current cause of ozone depletion in the stratosphere. To this date N_2O emissions are not actually regulated by the EU, however, this matter will definitely be of future interest. That said the development of selective catalytic systems to reduce NO_x emissions while using low-cost, non-noble metal-containing, catalytic systems is of great importance. Perovskite-based catalysts appear to be potential candidates for this purpose.

The low cost of perovskites combined with their unique physicochemical properties (i.e., redox/mixed valency properties of metals, O_2-mobility, and bulk and surface oxygen vacancies) and versatility of composition render this class of materials as great candidates for SCR of NO_x.

The easiness of substituting A and B-sites in ABO_3 and A_2BO_4 perovskite formulas with rare earth metals, alkali, or alkaline earth elements (at A-sites), and transition metals from the 3d, 4d, or 5d configuration (at B-sites), endows them with a variety of different active sites capable of facilitating the adsorption of the reactants on different sites, thus eliminating the catalytic rate inhibitory competitive adsorption of reactants on the same sites.

The incorporation of noble metals such as Pd into the B-site seems an interesting option to enhance catalytic performance since there is an increase in both cationic defects and lattice oxygen mobility. In addition, using perovskites as supporting materials in low NM-loading supported catalysts can provide benefits through metal-support interactions corroborated by the high reducibility and oxygen ion mobility and capacity characteristics of perovskites.

Several papers have been published on perovskite-catalyzed $C_xH_y/C_xH_yO_z$−, H_2−, and CO−SCR of NO_x. Most of these involved H_2−SCR, a few $C_xH_y/C_xH_yO_z$−SCR, and almost none CO−SCR. Representative cases of these works were analyzed in detail in this review and the achievements were presented comparatively in three comprehensive tables at the end of each respective section. For the sake of further convenience of comparison, the tables also include some results from NM-based catalysts applied under similar SCR conditions.

General conclusions that can be drawn and the corresponding perspectives are as follows:

- The SCR of NO_x behavior of perovskites (both in activity and N_2-selectivity) is comparable, if not better (especially at low temperatures) to that of NM-based catalysts. Their time-on-stream stability and SO_2 tolerance are also remarkable.
- The partial replacement of A and/or B-sites with other suitable elements allows a significant improvement and controlled optimization of their SCR performance. For example, partially substituted with Cu perovskites were found to be significantly more active in comparison with the bare sample, due to the additional effect of the advantageous in catalysis Cu^{2+}/Cu^{+} redox couple.
- Preparation methods capable of providing perovskites with a larger specific surface area are particularly advantageous due to the increased number of accessible active sites exposed to the reaction mixture. The typical specific surface of perovskites produced by traditional methods ranges between 5 and 20 $m^2 \cdot g^{-1}$. Advanced or modified classical methods have been reported which can raise these values by two or even three times resulting in a significant catalytic benefit during SCR of NO_x. Currently, significant efforts have been put to synthesize perovskites with surface areas as high as 100 $m^2 \cdot g^{-1}$.
- Extensive characterizations of the synthesized perovskite materials that were frequently applied allowed the researchers to better understand the reaction pathways, the nature, and the role of the active sites, thus extracting relatively reliable morphology–activity correlations. However, apart from the in situ DRIFTS studies, no other operando techniques such as in situ XRD and in situ TEM were found to have been applied to the studies included herein. In light of such shortcomings, the frequent

borrowing of reaction mechanisms from those proposed for analogous NM-based systems is justified. However, the use of perovskites in the SCR process is more likely to introduce new, easier reaction pathways that need to be in-depth understood in order to proceed with a coordinated optimization of perovskite composition for the SCR of NO_x. At the same time, DFT calculations that are generally missing from the documents included herein can be particularly helpful in the above objectives.

- On the other hand, modern approaches in catalysis have emerged following the pioneering work of the Hamada team [50] on what is now described as "*exsolution*" that offers new perspectives on the use of perovskites. The creation of different kinds of alloy or metal particles at nano or even atomic sizes on the surface of perovskites may provide the chance of tailoring the local surface properties and metal–support interactions, leading to enhanced performance. The active interfaces generated by the exsolution process can also result in higher activity and stability for this type of catalyst. The method could provide effective solutions in the field of SCR of NO_x as well. Due to the recency of the discovery, applications focused on the specific topic of this review have not yet been found (the work of Hamada and co-workers was implemented in TWC conditions). We could assume that the *exsolution* concept will be an intense research approach in the coming years on NO_x abatement under lean conditions.

It is obvious from the above that there is significant free space and many degrees of freedom for object research, which can bring significant environmental benefits and value. Perovskites as materials show unique handling properties and tailoring them through their composition could optimize SCR of NO_x. They are thermally stable, rather tolerant of poisons, and above all seem to work adequately with all possible reducing agents considered herein.

The specialized properties of perovskites, such as multiple types of active centers including surface oxygen vacancies, as well as labile lattice oxygen and mobile O^{2-} ions are particularly useful in catalysis. According to recent discoveries, these properties can play multiple roles as reaction promoters and as stabilizers of dispersed catalyst nanoparticles providing catalysts with high anti-sintering characteristics [26–30].

Even though the total exclusion of precious metals in catalytic processes seems unrealistic in the short run, combined use of both may provide substantial technological advantages. Based on the significant research carried out in this field, it can be argued that perovskites can serve as suitable active supports for precious metals, allowing both the reduction of noble metal loadings and the extension of their lifetime, bearing in mind the issues mentioned in the above paragraph.

As has been shown, the deNO_x efficacy of perovskites is remarkable for all the reducing agents considered herein. This provides additional practical benefits and alternatives. We believe that the involvement of perovskites in SCR of NO_x could further expand the Environmental Catalysis Society's potential for a cleaner environment, although catalysis has virtually unlimited outlets. More efforts are needed in fundamental and application studies for deNO_x processes catalyzed by perovskites to fully enhance their potential in the field—there is ample open space for promising research and development on the subject.

Author Contributions: I.V.Y.: Conceptualization, Data curation, Investigation, Writing—original draft, Writing—Review and editing, Project administration, Funding acquisition; A.G.G.: Conceptualization, Data curation, Investigation, Writing—original draft; C.D.: Data curation, Investigation, Writing—Review and editing; N.D.C.: Conceptualization, Writing—Review and editing; M.A.G.: Writing—Review and editing, Project administration, Funding acquisition. All authors have read and agreed to the published version of the manuscript.

Funding: The authors gratefully acknowledge that this research has been co-financed by the European Union and Greek national funds under the call "Greece–China Call for Proposals for Joint RT&D Projects". Project title: Development of new Catalysts for Efficient De-NO_x Abatement of Automobile Exhaust Purification (Project code: T7DKI-00356).

Institutional Review Board Statement: Not applicable.

Informed Consent Statement: Not applicable.

Data Availability Statement: No new data were created or analyzed in this study. Data sharing is not applicable to this article.

Conflicts of Interest: The authors declare no conflict of interest.

Abbreviations

BET	Brunauer, Emmett and Teller
CBM	Coal Bed Methane
DFT	Density Functional Theory
DLS	Dynamic Light Scattering
DRIFTS	Diffuse Reflectance Infrared Fourier Transform Spectroscopy
DSC	Differential Scanning Calorimetry
EDS	Energy-Dispersive X-ray Spectroscopy
EF-TEM	Energy Filtering Transmission Electron Microscopy
FE-SEM	Field Emission Scanning Electron Microscopy
FTIR	Fourier Transform Infrared Spectroscopy
HCs	Hydrocarbons
ICP-AES	Inductively Coupled Plasma Atomic Emission Spectroscopy
ICP-OES	Inductively Coupled Plasma Optical Emission Spectroscopy
PM	Particulate Matter
SCR	Selective Catalytic Reduction
SEM	Scanning Electron Microscopy
TEM	Transmission Electron Microscopy
TPD	Temperature-Programmed Desorption
TPR	Temperature-Programmed Reduction
TWC	Three-Way Catalysts
WGHSV	Weight-basis Gas Hourly Space Velocity
XRD	X-ray Diffraction
XPS	X-ray Photoelectron Spectroscopy

References

1. Granger, P.; Parvulescu, V.I. Catalytic NOx abatement systems for mobile sources: From three-way to lean burn after-treatment technologies. *Chem. Rev.* **2011**, *111*, 3155–3207. https://doi.org/10.1021/cr100168g.
2. Yentekakis, I.V.; Konsolakis, M. Three-way Catalysis. In *Perovskites and Related Mixed Oxides*; Wiley-VCH, Vergal GmbH & Co. KGaA: Weinheim, Germany, **2016**; pp. 559–586. https://doi.org/10.1002/9783527686605.ch25.
3. Yentekakis, I.V.; Vernoux, P. Emissions control catalysis. *Catalysts* **2019**, *9*, 912. https://doi.org/10.3390/catal9110912.
4. Yentekakis, I.V.; Vernoux, P.; Goula, G.; Caravaca, A. Electropositive promotion by Alkalis or Alkaline earths of Pt-group metals in emissions control catalysis: A status report. *Catalysts* **2019**, *9*, 157. https://doi.org/10.3390/catal9020157.
5. Yentekakis, I.V.; Dong, F. Grand Challenges for Catalytic Remediation in Environmental and Energy Applications Toward a Cleaner and Sustainable Future. *Front. Environ. Chem.* **2020**, *1*, 5. https://doi.org/10.3389/fenvc.2020.00005.
6. Damma, D.; Ettireddy, P.R.; Reddy, B.M.; Smirniotis, P.G. A review of low temperature NH_3-SCR for removal of NOx. *Catalysts* **2019**, *9*, 349. https://doi.org/10.3390/catal9040349.
7. Yentekakis, I.V.; Tellou, V.; Botzolaki, G.; Rapakousios, I.A. A comparative study of the C_3H_6 + NO + O_2, C_3H_6 + O_2 and NO + O_2 reactions in excess oxygen over Na-modified Pt/γ-Al_2O_3 catalysts. *Appl. Catal. B Environ.* **2005**, *56*, 229–239. https://doi.org/10.1016/j.apcatb.2004.08.017.
8. Goula, M.A.; Charisiou, N.D.; Papageridis, K.N.; Delimitis, A.; Papista, E.; Pachatouridou, E.; Iliopoulou, E.F.; Marnellos, G.; Konsolakis, M.; Yentekakis, I.V. A comparative study of the H_2-assisted selective catalytic reduction of nitric oxide by propene over noble metal (Pt, Pd, Ir)/γ-Al_2O_3 catalysts. *J. Environ. Chem. Eng.* **2016**, *4*, 1629–1641. https://doi.org/10.1016/j.jece.2016.02.025.
9. Costa, C.N.; Savva, P.G.; Andronikou, C.; Lambrou, P.S.; Polychronopoulou, K.; Belessi, V.C.; Stathopoulos, V.N.; Pomonis, P.J.; Efstathiou, A.M. An investigation of the NO/H_2/O_2 (Lean De-NOx) reaction on a highly active and selective Pt/$La_{0.7}Sr_{0.2}Ce_{0.1}FeO_3$ catalyst at low temperatures. *J. Catal.* **2002**, *209*, 456–471. https://doi.org/10.1006/jcat.2002.3645.
10. Polychronopoulou, K.; Efstathiou, A.M. NOx Control via H_2-Selective Catalytic Reduction (H_2-SCR) Technology for Stationary and Mobile Applications. *Recent Patents Mater. Sci.* **2012**, *5*, 84–107. https://doi.org/10.2174/1874465611205020087.

11. Machida, M.; Ikeda, S.; Kurogi, D.; Kijima, T. Low temperature catalytic NOx–H_2 reactions over Pt/TiO_2-ZrO_2 in an excess oxygen. *Appl. Catal. B Environ.* **2001**, *35*, 107–116. https://doi.org/10.1016/S0926-3373(01)00243-0.
12. Macleod, N.; Lambert, R.M. An in situ DRIFTS study of efficient lean NOx reduction with H_2 + CO over Pd/Al_2O_3: The key role of transient NCO formation in the subsequent generation of ammonia. *Appl. Catal. B Environ.* **2003**, *46*, 483–495. https://doi.org/10.1016/S0926-3373(03)00289-3.
13. Konsolakis, M.; Vrontaki, M.; Avgouropoulos, G.; Ioannides, T.; Yentekakis, I.V. Novel doubly-promoted catalysts for the lean NOx reduction by H_2 + CO: Pd(K)/Al_2O_3–(TiO_2). *Appl. Catal. B Environ.* **2006**, *68*, 59–67. https://doi.org/10.1016/j.apcatb.2006.07.011.
14. Pekridis, G.; Kaklidis, N.; Komvokis, V.; Athanasiou, C.; Konsolakis, M.; Yentekakis, I.V.; Marnellos, G.E. Surface and catalytic elucidation of Rh/γ-Al_2O_3 catalysts during NO reduction by C_3H_8 in the presence of excess O_2, H_2O, and SO_2. *J. Phys. Chem. A* **2010**, *114*, 3969–3980. https://doi.org/10.1021/jp907589c.
15. Burch, R. Knowledge and know-how in emission control for mobile applications. *Catal. Rev. Sci. Eng.* **2004**, *46*, 271–334. https://doi.org/10.1081/CR-200036718.
16. Macleod, N.; Isaac, J.; Lambert, R.M. Sodium Promotion of the NO+C_3H_6 Reaction over Rh/γ-Al_2O_3 Catalysts. *J. Catal.* **2000**, *193*, 115–122. https://doi.org/10.1006/jcat.2000.2882.
17. Yentekakis, I.V.; Konsolakis, M.; Rapakousios, I.A.; Matsouka, V. Novel electropositively promoted monometallic (Pt-only) catalytic converters for automotive pollution control. *Top. Catal.* **2007**, *42–43*, 393–397. https://doi.org/10.1007/s11244-007-0212-0.
18. Yentekakis, I.V.; Lambert, R.M.; Konsolakis, M.; Kiousis, V. The effect of sodium on the Pd-catalyzed reduction of NO by methane. *Appl. Catal. B Environ.* **1998**, *18*, 293–305. https://doi.org/10.1016/S0926-3373(98)00049-6.
19. Konsolakis, M.; Yentekakis, I.V. Strong promotional effects of Li, K, Rb and Cs on the Pt-catalysed reduction of NO by propene. *Appl. Catal. B Environ.* **2001**, *29*, 103–113. https://doi.org/10.1016/S0926-3373(00)00195-8.
20. Konsolakis, M.; Yentekakis, I.V. The reduction of NO by propene over Ba-promoted Pt/γ-Al_2O_3 catalysts. *J. Catal.* **2001**, *198*, 142–150. https://doi.org/10.1006/jcat.2000.3123.
21. Tanikawa, K.; Egawa, C. Effect of barium addition over palladium catalyst for CO-NO-O_2 reaction. *J. Mol. Catal. A Chem.* **2011**, *349*, 94–99. https://doi.org/10.1016/j.molcata.2011.08.025.
22. Palermo, A.; Lambert, R.M.; Harkness, I.R.; Yentekakis, I.V.; Marina, O.; Vayenas, C.G. Electrochemical promotion by Na of the platinum-catalyzed reaction between CO and NO. *J. Catal.* **1996**, *161*, 471–479. https://doi.org/10.1006/jcat.1996.0206.
23. Papadakis, V.G.; Pliangos, C.A.; Yentekakis, I.V.; Verykios, X.E.; Vayenas, C.G. Development of high performance, Pd-based, three-way catalysts. *Catal. Today* **1996**, *29*, 71–75. https://doi.org/10.1016/0920-5861(95)00268-5.
24. Palermo, A.; Tikhov, M.S.; Filkin, N.C.; Lambert, R.M.; Yentekakis, I.V.; Vayenas, C.G. Electrochemical promotion of NO reduction by CO and by propene. *Stud. Surf. Sci. Catal.* **1996**, *101*, 513–522. https://doi.org/10.1016/S0167-2991(96)80262-X.
25. Matsouka, V.; Konsolakis, M.; Yentekakis, I.V.; Papavasiliou, A.; Tsetsekou, A.; Boukos, N. Thermal aging behavior of Pt-only TWC converters under simulated exhaust conditions: Effect of rare earths (CeO_2, La_2O_3) and alkali (Na) modifiers. *Top. Catal.* **2011**, *54*, 1124–1134. https://doi.org/10.1007/s11244-011-9734-6.
26. Yentekakis, I.V.; Goula, G.; Panagiotopoulou, P.; Kampouri, S.; Taylor, M.J.; Kyriakou, G.; Lambert, R.M. Stabilization of catalyst particles against sintering on oxide supports with high oxygen ion lability exemplified by Ir-catalyzed decomposition of N_2O. *Appl. Catal. B Environ.* **2016**, *192*, 357–364. https://doi.org/10.1016/j.apcatb.2016.04.011.
27. Yentekakis, I.V.; Goula, G.; Kampouri, S.; Betsi-Argyropoulou, I.; Panagiotopoulou, P.; Taylor, M.J.; Kyriakou, G.; Lambert, R.M. Ir-Catalysed Nitrous oxide (N_2O) Decomposition: Effect of Ir Particle Size and Metal–Support Inter-actions. *Catal. Letters* **2018**, *148*, 341–347. https://doi.org/10.1007/s10562-017-2233-z.
28. Yentekakis, I.V.; Goula, G.; Panagiotopoulou, P.; Katsoni, A.; Diamadopoulos, E.; Mantzavinos, D.; Delimitis, A. Dry reforming of methane: Catalytic performance and stability of Ir catalysts supported on γ-Al_2O_3, $Zr_{0.92}Y_{0.08}O_{2-\delta}$ (YSZ) or $Ce_{0.9}Gd_{0.1}O_{2-\delta}$ (GDC) supports. *Top. Catal.* **2015**, *58*, 1228–1241. https://doi.org/10.1007/s11244-015-0490-x.
29. Goula, G.; Botzolaki, G.; Osatiashtiani, A.; Parlett, C.M.A.; Kyriakou, G.; Lambert, R.M.; Yentekakis, I.V. Oxidative thermal sintering and redispersion of Rh nanoparticles on supports with high oxygen ion lability. *Catalysts* **2019**, *9*, 541. https://doi.org/10.3390/catal9060541.
30. Nikolaraki, E.; Goula, G.; Panagiotopoulou, P.; Taylor, M.J.; Kousi, K.; Kyriakou, G.; Kondarides, D.I.; Lambert, R.M.; Yentekakis, I.V. Support induced effects on the Ir nanoparticles activity, selectivity and stability performance under CO_2 reforming of methane. *Nanomaterials* **2021**, *11*, 2880. https://doi.org/10.3390/nano11112880.
31. Granger, P.; Parvulescu, V.I.; Kaliaguine, S.; Prellier, W. *Perovskites and Related Mixed Oxides*; Granger, P., Parvulescu, V.I., Kaliaguine, S., Prellier, W., Eds.; Wiley-VCH, Vergal GmbH & Co. KGaA: Weinheim, Germany, **2016**; Volumes 1 and 2; ISBN 978-3-527-33763-7.
32. Zhu, J.; Li, H.; Zhong, L.; Xiao, P.; Xu, X.; Yang, X.; Zhao, Z.; Li, J. Perovskite oxides: Preparation, characterizations, and applications in heterogeneous catalysis. *ACS Catal.* **2014**, *4*, 2917–2940. https://doi.org/10.1021/cs500606g.
33. Royer, S.; Duprez, D.; Can, F.; Courtois, X.; Batiot-Dupeyrat, C.; Laassiri, S.; Alamdari, H. Perovskites as substitutes of noble metals for heterogeneous catalysis: Dream or reality. *Chem. Rev.* **2014**, *114*, 10292–10368. https://doi.org/10.1021/cr500032a.
34. Hwang, J.; Rao, R.R.; Giordano, L.; Katayama, Y.; Yu, Y.; Shao-Horn, Y. Perovskites in catalysis and electrocatalysis. *Science* **2017**, *358*, 751–756. https://doi.org/10.1126/science.aam7092.

35. Tarjomannejad, A.; Niaei, A.; Gómez, M.J.I.; Farzi, A.; Salari, D.; Albaladejo-Fuentes, V. NO + CO reaction over $LaCu_{0.7}B_{0.3}O_3$ (B = Mn, Fe, Co) and $La_{0.8}A_{0.2}Cu_{0.7}Mn_{0.3}O_3$ (A = Rb, Sr, Cs, Ba) perovskite-type catalysts. *J. Therm. Anal. Calorim.* **2017**, *129*, 671–680. https://doi.org/10.1007/s10973-017-6264-x.
36. Bhattar, S.; Abedin, M.A.; Kanitkar, S.; Spivey, J.J. A review on dry reforming of methane over perovskite derived catalysts. *Catal. Today* **2021**, *365*, 2–23. https://doi.org/10.1016/j.cattod.2020.10.041.
37. Sim, Y.; Kwon, D.; An, S.; Ha, J.M.; Oh, T.S.; Jung, J.C. Catalytic behavior of ABO3 perovskites in the oxidative coupling of methane. *Mol. Catal.* **2020**, *489*, 110925. https://doi.org/10.1016/j.mcat.2020.110925.
38. Yang, E.-h.; Noh, Y.S.; Hong, G.H.; Moon, D.J. Combined steam and CO_2 reforming of methane over $La_{1-x}Sr_xNiO_3$ perovskite oxides. *Catal. Today* **2018**, *299*, 242–250. https://doi.org/10.1016/j.cattod.2017.03.050.
39. Lima, S.M.; Assaf, J.M.; Peña, M.A.; Fierro, J.L.G. Structural features of $La_{1-x}Ce_xNiO_3$ mixed oxides and performance for the dry reforming of methane. *Appl. Catal. A Gen.* **2006**, *311*, 94–104. https://doi.org/10.1016/j.apcata.2006.06.010.
40. Wang, M.; Zhao, T.; Dong, X.; Li, M.; Wang, H. Effects of Ce substitution at the A-site of $LaNi_{0.5}Fe_{0.5}O_3$ perovskite on the enhanced catalytic activity for dry reforming of methane. *Appl. Catal. B Environ.* **2018**, *224*, 214–221. https://doi.org/10.1016/j.apcatb.2017.10.022.
41. Peña, M.A.; Fierro, J.L.G. Chemical structures and performance of perovskite oxides. *Chem. Rev.* **2001**, *101*, 1981–2017. https://doi.org/10.1021/cr980129f.
42. Shen, M.; Zhao, Z.; Chen, J.; Su, Y.; Wang, J.; Wang, X. Effects of calcium substitute in $LaMnO_3$ perovskites for NO catalytic oxidation. *J. Rare Earths* **2013**, *31*, 119–123. https://doi.org/10.1016/S1002-0721(12)60244-0.
43. Zhang, R.; Villanueva, A.; Alamdari, H.; Kaliaguine, S. Reduction of NO by CO over nanoscale $LaCo_{1-x}Cu_xO_3$ and $LaMn_{1-x}Cu_xO_3$ perovskites. *J. Mol. Catal. A Chem.* **2006**, *258*, 22–34. https://doi.org/10.1016/j.molcata.2006.05.008.
44. Misono, M. A view on the future of mixed oxide catalysts: The case of heteropolyacids (polyoxometalates) and perovskites. *Catal. Today* **2005**, *100*, 95–100. https://doi.org/10.1016/j.cattod.2004.12.010.
45. Yentekakis, I.V. Open- and closed-circuit study of an intermediate temperature SOFC directly fueled with simulated biogas mixtures. *J. Power Sources* **2006**, *29*, 422–425. https://doi.org/10.1016/j.jpowsour.2005.12.069.
46. Yentekakis, I.V.; Papadam, T.; Goula, G. Electricity production from wastewater treatment via a novel biogas-SOFC aided process. *Solid State Ionics* **2008**, *179*, 1521–1525. https://doi.org/10.1016/j.ssi.2007.12.049.
47. Buciuman, F.-C.; Joubert, E.; Menezo, J.-C.; Barbier, J. Catalytic properties of $La_{0.8}A_{0.2}MnO_3$ (A = Sr, Ba, K, Cs) and $LaMn_{0.8}B_{0.2}O_3$ (B = Ni, Zn, Cu) perovskites. *Appl. Catal. B Environ.* **2001**, *35*, 149–156. https://doi.org/10.1016/s0926-3373(01)00249-1.
48. Wu, X.; Xu, L.; Weng, D. The NO selective reduction on the $La_{1-x}Sr_xMnO_3$ catalysts. *Catal. Today* **2004**, *90*, 199–206. https://doi.org/10.1016/j.cattod.2004.04.027.
49. Kousi, K.; Tang, C.; Metcalfe, I.S.; Neagu, D. Emergence and future of exsolved materials. *Small* **2021**, *17*, 2006479. https://doi.org/10.1002/smll.202006479.
50. Nishihata, Y.; Mizuki, J.; Akao, T.; Tanaka, H.; Uenishi, M.; Kimura, M.; Okamoto, T.; Hamada, N. Self-regeneration of a Pd-perovskite catalyst for automotive emissions control. *Nature* **2002**, *418*, 164–167. https://doi.org/10.1038/nature00893.
51. Kwon, O.; Joo, S.; Choi, S.; Sengodan, S.; Kim, G. Review on exsolution and its driving forces in perovskites. *J. Phys Energy* **2020**, *2*, 032001. https://doi.org/10.1088/2515-7655/ab8c1f.
52. He, H.; Dai, H.X.; Au, C.T. An investigation on the utilization of perovskite-type oxides $La_{1-x}Sr_xMO_3$ (M = $Co_{0.77}Bi_{0.20}Pd_{0.03}$) as three-way catalysts. *Appl. Catal. B Environ.* **2001**, *33*, 65–80. https://doi.org/10.1016/S0926-3373(01)00159-X.
53. Zhu, J.; Zhao, Z.; Xiao, D.; Li, J.; Yang, X.; Wu, Y. Study of $La_{2-x}Sr_xCuO_4$ (x = 0.0, 0.5, 1.0) catalysts for NO + CO reaction from the measurements of O_2-TPD, H_2-TPR and cyclic voltammetry. *J. Mol. Catal. A Chem.* **2005**, *238*, 35–40. https://doi.org/10.1016/j.molcata.2005.03.036.
54. Fino, D.; Fino, P.; Saracco, G.; Specchia, V. Studies on kinetics and reactions mechanism of $La_{2-x}K_xCu_{1-y}VyO_4$ layered perovskites for the combined removal of diesel particulate and NOx. *Appl. Catal. B Environ.* **2003**, *43*, 243–259. https://doi.org/10.1016/S0926-3373(02)00311-9.
55. Centi, G.; Perathoner, S. Nature of active species in copper-based catalysts and their chemistry of transformation of nitrogen oxides. *Appl. Catal. A Gen.* **1995**, *132*, 179–259. https://doi.org/10.1016/0926-860X(95)00154-9.
56. Yahiro, H.; Iwamoto, M. Copper ion-exchanged zeolite catalysts in deNOx reaction. *Appl. Catal. A Gen.* **2001**, *222*, 163–181. https://doi.org/10.1016/S0926-860X(01)00823-7.
57. Zhang, R.; Villanueva, A.; Alamdari, H.; Kaliaguine, S. Catalytic reduction of NO by propene over $LaCo_{1-x}Cu_xO_3$ perovskites synthesized by reactive grinding. *Appl. Catal. B Environ.* **2006**, *64*, 220–233. https://doi.org/10.1016/j.apcatb.2005.10.028.
58. Zhang, R.; Villanueva, A.; Alamdari, H.; Kaliaguine, S. SCR of NO by propene over nanoscale $LaMn_{1-x}Cu_xO_3$ perovskites. *Appl. Catal. A Gen.* **2006**, *307*, 85–97. https://doi.org/10.1016/j.apcata.2006.03.019.
59. Glisenti, A.; Pacella, M.; Guiotto, M.; Natile, M.M.; Canu, P. Largely Cu-doped $LaCo_{1-x}Cu_xO_3$ perovskites for TWC: Toward new PGM-free catalysts. *Appl. Catal. B Environ.* **2016**, *180*, 94–105. https://doi.org/10.1016/j.apcatb.2015.06.017.
60. Levasseur, B.; Kaliaguine, S. Effects of iron and cerium in $La_{1-y}Ce_yCo_{1-x}Fe_xO_3$ perovskites as catalysts for VOC oxidation. *Appl. Catal. B Environ.* **2009**, *88*, 305–314. https://doi.org/10.1016/j.apcatb.2008.11.007.
61. Deng, C.; Huang, Q.; Zhu, X.; Hu, Q.; Su, W.; Qian, J.; Dong, L.; Li, B.; Fan, M.; Liang, C. The influence of Mn-doped CeO_2 on the activity of CuO/CeO_2 in CO oxidation and NO + CO model reaction. *Appl. Surf. Sci.* **2016**, *389*, 1033–1049. https://doi.org/10.1016/j.apsusc.2016.08.035.

62. Deng, C.; Qian, J.; Yu, C.; Yi, Y.; Zhang, P.; Li, W.; Dong, L.; Li, B.; Fan, M. Influences of doping and thermal stability on the catalytic performance of CuO/$Ce_{20}M_{1O_x}$ (M = Zr, Cr, Mn, Fe, Co, Sn) catalysts for NO reduction by CO. *RSC Adv.* **2016**, *6*, 113630–113647. https://doi.org/10.1039/c6ra21740k.
63. Ma, J.; Jin, G.; Gao, J.; Li, Y.; Dong, L.; Huang, M.; Huang, Q.; Li, B. Catalytic effect of two-phase intergrowth and coexistence CuO-CeO_2. *J. Mater. Chem. A* **2015**, *3*, 24358–24370. https://doi.org/10.1039/c5ta06435j.
64. Giannakas, A.E.; Leontiou, A.A.; Ladavos, A.K.; Pomonis, P.J. Characterization and catalytic investigation of NO + CO reaction on perovskites of the general formula $La_xM_{1-x}FeO_3$ (M = Sr and/or Ce) prepared via a reverse micelles microemulsion route. *Appl. Catal. A Gen.* **2006**, *309*, 254–262. https://doi.org/10.1016/j.apcata.2006.05.016.
65. Costa, C.N.; Efstathiou, A.M. Low-temperature H_2-SCR of NO on a novel Pt/MgO-CeO_2 catalyst. *Appl. Catal. B Environ.* **2007**, *72*, 240–252. https://doi.org/10.1016/j.apcatb.2006.11.010.
66. Engelmann-Pirez, M.; Granger, P.; Leclercq, G. Investigation of the catalytic performances of supported noble metal based catalysts in the NO + H_2 reaction under lean conditions. *Catal. Today* **2005**, *107–108*, 315–322. https://doi.org/10.1016/j.cattod.2005.07.087.
67. Mondragón Rodríguez, G.C.; Saruhan, B. Effect of Fe/Co-ratio on the phase composition of Pd-integrated perovskites and its H_2-SCR of NOx performance. *Appl. Catal. B Environ.* **2010**, *93*, 304–313. https://doi.org/10.1016/j.apcatb.2009.10.004.
68. Sato, S.; Yu-u, Y.; Yahiro, H.; Mizuno, N.; Iwamoto, M. Cu-ZSM-5 zeolite as highly active catalyst for removal of nitrogen monoxide from emission of diesel engines. *Appl. Catal.* **1991**, *70*, 3–7. https://doi.org/10.1016/S0166-9834(00)84146-9.
69. Vasala, S.; Karppinen, M. $A_2B'B''O_6$ perovskites: A review. *Prog. Solid State Chem.* **2015**, *43*, 1–36. https://doi.org/10.1016/j.progsolidstchem.2014.08.001.
70. Li, X.; Chen, C.; Liu, C.; Xian, H.; Guo, L.; Lv, J.; Jiang, Z. Pd-Doped Perovskite: An Effective Catalyst for Removal of NO. *ACS Catal.* **2013**, *3*, 1071–1075. https://doi.org/10.1021/cs400136t.
71. Kucherov, A.V.; Gerlock, J.L.; Jen, H.W.; Shelef, M. In Situ ESR Monitoring of CuH-ZSM-5 Up to 500 °C in Flowing Dry Mixtures of NO(NO_2), C_3H_6(C_2H_5OH), and Excess O_2. *J. Catal.* **1995**, *152*, 63–69. https://doi.org/10.1006/jcat.1995.1060.
72. Ukisu, Y.; Miyadera, T.; Abe, A.; Yoshida, K. Infrared study of catalytic reduction of lean NOx with alcohols over alumina-supported silver catalyst. *Catal. Letters* **1996**, *39*, 265–267. https://doi.org/10.1007/BF00805593.
73. Wu, Q.; He, H.; Yu, Y. In situ DRIFTS study of the selective reduction of NOx with alcohols over Ag/Al_2O_3 catalyst: Role of surface enolic species. *Appl. Catal. B Environ.* **2005**, *61*, 107–113. https://doi.org/10.1016/j.apcatb.2005.04.012.
74. Wang, H.; Zhang, R.; Li, P.; Royer, S.; Dacquin, J.P. Mechanistic insight into the methanol selective catalytic reduction of NO reaction over Cu-containing perovskites. *J. Catal.* **2019**, *377*, 480–493. https://doi.org/10.1016/j.jcat.2019.07.035.
75. Teng, Z.; Huang, S.; Zhang, H.; Yu, H.; Li, N.; Zhou, Q. A system including enriching coal bed methane by solar energy and selective catalytic reduction. *Appl. Therm. Eng.* **2018**, *130*, 822–829. https://doi.org/10.1016/j.applthermaleng.2017.11.058.
76. Teng, Z.; Zhang, H.; Huang, S.; Li, N.; Zhou, Q. Experimental study on reduction of NO by CH_4 over $La_{0.8}Sr_{0.2}MnO_3$/α-Al_2O_3 in excess of O_2. *J. Taiwan Inst. Chem. Eng.* **2018**, *87*, 204–210. https://doi.org/10.1016/j.jtice.2018.03.036.
77. Giroir-Fendler, A.; Gil, S.; Baylet, A. ($La_{0.8}A_{0.2}$)MnO_3 (A = Sr, K) perovskite catalysts for NO and $C_{10}H_{22}$ oxidation and selective reduction of NO by $C_{10}H_{22}$. *Cuihua Xuebao / Chinese J. Catal.* **2014**, *35*, 1299–1304. https://doi.org/10.1016/S1872-2067(14)60173-X.
78. Tabata, K.; Hirano, Y.; Suzuki, E. XPS studies on the oxygen species of $LaMn_{1-x}Cu_xO_{3+\lambda}$. *Appl. Catal. A Gen.* **1998**, *170*, 245–254. https://doi.org/10.1016/S0926-860X(98)00062-3.
79. Baylet, A.; Royer, S.; Labrugère, C.; Valencia, H.; Marécot, P.; Tatibouët, J.M.; Duprez, D. Effect of palladium on the reducibility of Mn based materials: Correlation with methane oxidation activity. *Phys. Chem. Chem. Phys.* **2008**, *10*, 5983–5992. https://doi.org/10.1039/b808289h.
80. Luo, Y.; Wang, X.; Qian, Q.; Chen, Q. Studies on B sites in Fe-doped $LaNiO_3$ perovskite for SCR of NOx with H_2. *Int. J. Hydrogen Energy* **2014**, *39*, 15836–15843. https://doi.org/10.1016/j.ijhydene.2014.07.135.
81. Furfori, S.; Russo, N.; Fino, D.; Saracco, G.; Specchia, V. NO SCR reduction by hydrogen generated in line on perovskite-type catalysts for automotive diesel exhaust gas treatment. *Chem. Eng. Sci.* **2010**, *65*, 120–127. https://doi.org/10.1016/j.ces.2009.01.065.
82. Burch, R.; Coleman, M.D. An investigation of the NO/H_2/O_2 reaction on noble-metal catalysts at low temperatures under lean-burn conditions. *Appl. Catal. B Environ.* **1999**, *23*, 115–121. https://doi.org/10.1016/S0926-3373(99)00073-9.
83. Dhainaut, F.; Pietrzyk, S.; Granger, P. Kinetic investigation of the NO reduction by H_2 over noble metal based catalysts. *Catal. Today* **2007**, *119*, 94–99. https://doi.org/10.1016/j.cattod.2006.08.016.
84. Barrera, A.; Viniegra, M.; Bosch, P.; Lara, V.H.; Fuentes, S. Pd/Al_2O_3-La_2O_3 catalysts prepared by sol-gel: Characterization and catalytic activity in the NO reduction by H_2. *Appl. Catal. B Environ.* **2001**, *34*, 97–111. https://doi.org/10.1016/S0926-3373(01)00206-5.
85. Mondragon Rodriguez, G.C.; Kelm, K.; Saruhan, B. H_2-selective catalytic reduction of NOx activity and microstructural analysis of new $BaTi_{0.9}5Pd_{0.0}5O_3$ catalyst. *Appl. Catal. A Gen.* **2010**, *387*, 173–184. https://doi.org/10.1016/j.apcata.2010.08.012.
86. Costa, C.N.; Efstathiou, A.M.; Stathopoulos, V.N.; Belessi, V.C. An investigation of the NO/H_2/O_2 (Lean-deNOx) reaction on a highly active and selective Pt/$La_{0.5}Ce_{0.5}MnO_3$ catalyst. *J. Catal.* **2001**, *197*, 350–364. https://doi.org/10.1006/jcat.2000.3101.
87. Macleod, N.; Lambert, R.M. Lean NOx reduction with CO + H_2 mixtures over Pt/Al_2O_3 and Pd/Al_2O_3 catalysts. *Appl. Catal. B Environ.* **2002**, *35*, 269–279. https://doi.org/10.1016/S0926-3373(01)00264-8.
88. Dhainaut, F.; Pietrzyk, S.; Granger, P. NO + H_2 reaction on Pd/Al_2O_3 under lean conditions: Kinetic study. *Top. Catal.* **2007**, *42–43*, 135–141. https://doi.org/10.1007/s11244-007-0166-2.

89. Matsouka, V.; Konsolakis, M.; Lambert, R.M.; Yentekakis, I.V. In situ DRIFTS study of the effect of structure (CeO_2–La_2O_3) and surface (Na) modifiers on the catalytic and surface behaviour of Pt/γ-Al_2O_3 catalyst under simulated exhaust conditions. *Appl. Catal. B Environ.* **2008**, *84*, 715-722. https://doi.org/10.1016/j.apcatb.2008.06.004.
90. Qin, Y.; Sun, L.; Zhang, D.; Huang, L. Role of ceria in the improvement of SO_2 resistance of $La_xCe_{1-x}FeO_3$ catalysts for catalytic reduction of NO with CO. *Catal. Commun.* **2016**, *79*, 53–57. https://doi.org/10.1016/j.catcom.2016.03.005.
91. Wu, Y.; Liu, H.; Li, G.; Jin, L.; Li, X.; Ou, X.; Dong, L.; Jin, G.; Li, B. Tuning composition on B sites of $LaM_{0.5}Mn_{0.5}O_3$ (M = Cu, Co, Fe, Ni, Cr) perovskite catalysts in NOx efficient reduction. *Appl. Surf. Sci.* **2020**, *508*, 145158. https://doi.org/10.1016/j.apsusc.2019.145158.
92. Wu, Y.; Chu, B.; Zhang, M.; Yi, Y.; Dong, L.; Fan, M.; Jin, G.; Zhang, L.; Li, B. Influence of calcination temperature on the catalytic properties of $LaCu_{0.25}Co_{0.75}O_3$ catalysts in NOx reduction. *Appl. Surf. Sci.* **2019**, *481*, 1277–1286. https://doi.org/10.1016/j.apsusc.2019.03.263.
93. Wu, Y.; Li, G.; Chu, B.; Dong, L.; Tong, Z.; He, H.; Zhang, L.; Fan, M.; Li, B.; Dong, L. NO Reduction by CO over Highly Active and Stable Perovskite Oxide Catalysts $La_{0.8}Ce_{0.2}M_{0.25}Co_{0.75}O_3$ (M = Cu, Mn, Fe): Effect of the Role in B Site. *Ind. Eng. Chem. Res.* **2018**, *57*, 15670–15682. https://doi.org/10.1021/acs.iecr.8b04214.
94. Yi, Y.; Liu, H.; Chu, B.; Qin, Z.; Dong, L.; He, H.; Tang, C.; Fan, M.; Bin, L. Catalytic removal NO by CO over La-$Ni_{0.5}M_{0.5}O_3$ (M = Co, Mn, Cu) perovskite oxide catalysts: Tune surface chemical composition to improve N_2 selectivity. *Chem. Eng. J.* **2019**, *369*, 511–521. https://doi.org/10.1016/j.cej.2019.03.066.
95. Tarjomannejad, A.; Farzi, A.; Gómez, M.J.I.; Niaei, A.; Salari, D.; Albaladejo-Fuentes, V. Catalytic Reduction of NO by CO over $LaMn_{1-x}Fe_xO_3$ and $La_{0.8}A_{0.2}Mn_{0.3}Fe_{0.7}O_3$ (A = Sr, Cs, Ba, Ce) Perovskite Catalysts. *Catal. Letters* **2016**, *146*, 2330–2340. https://doi.org/10.1007/s10562-016-1860-0.
96. Tarjomannejad, A.; Farzi, A.; Niaei, A.; Salari, D. NO reduction by CO over $LaB_{0.5}B'_{0.5}O_3$ (B = Fe, Mn, B′ = Fe, Mn, Co, Cu) perovskite catalysts, an experimental and kinetic study. *J. Taiwan Inst. Chem. Eng.* **2017**, *78*, 200–211. https://doi.org/10.1016/j.jtice.2017.05.034.
97. Lorimer, D.; Bell, A.T. Reduction of NO by CO over a silica-supported platinum catalyst: Infrared and kinetic studies. *J. Catal.* **1979**, *59*, 223–238. https://doi.org/10.1016/S0021-9517(79)80027-5.
98. Zhdanov, V.P.; Kasemo, B. Mechanism and kinetics of the NO-CO reaction on Rh. *Surf. Sci. Rep.* **1997**, *29*, 31–33. https://doi.org/10.1016/S0167-5729(97)00009-5.
99. de Lima, R.K.C.; Batista, M.S.; Wallau, M.; Sanches, E.A.; Mascarenhas, Y.P.; Urquieta-González, E.A. High specific surface area LaFeCo perovskites-Synthesis by nanocasting and catalytic behavior in the reduction of NO with CO. *Appl. Catal. B Environ.* **2009**, *90*, 441–450. https://doi.org/10.1016/j.apcatb.2009.04.004.
100. Giannakas, A.E.; Ladavos, A.K.; Pomonis, P.J. Preparation, characterization and investigation of catalytic activity for NO + CO reaction of $LaMnO_3$ and $LaFeO_3$ perovskites prepared via microemulsion method. *Appl. Catal. B Environ.* **2004**, *49*, 147–158. https://doi.org/10.1016/j.apcatb.2003.12.002.
101. Leontiou, A.A.; Ladavos, A.K.; Armatas, G.S.; Trikalitis, P.N.; Pomonis, P.J. Kinetics investigation of NO + CO reaction on La-Sr-Mn-O perovskite-type mixed oxides. *Appl. Catal. A Gen.* **2004**, *263*, 227–239. https://doi.org/10.1016/j.apcata.2003.12.017.
102. Konsolakis, M.; Yentekakis, I.V.; Palermo, A.; Lambert, R.M. Optimal promotion by rubidium of the CO + NO reaction over Pt/γ-Al_2O_3 catalysts. *Appl. Catal. B: Environ.* **2001**, *33*, 293–302. https://doi.org/10.1016/S0926-3373(01)00183-7.